SAND2019-7499PE

Measurement of Shock and Detonation Propagation Along Pentaerythritol Tetranitrate (PETN) Thin Films

Julio C. Peguero

Mechanical Engineering

NEW MEXICO TECH
SCIENCE • ENGINEERING • RESEARCH UNIVERSITY

Sandia National Laboratories

U.S. DEPARTMENT OF ENERGY
National Nuclear Security Administration

Sandia National Laboratories is a multimission laboratory managed and operated by National Technology & Engineering Solutions of Sandia, LLC, a wholly owned subsidiary of Honeywell International Inc., for the U.S. Department of Energy's National Nuclear Security Administration under contract DE-NA0003525.
Unclassified, unlimited release SAND2019-7499 PE

Outline

- Background and introduction
  - Physical vapor deposition (PVD) of explosives
  - Detonation failure
- Experimental methods
- Experimental results
- Computational methods
- Computational results
- Conclusions

Physical Vapor Deposition (PVD)

- PVD is a process used to deposit thin films of elements, compounds or molecules.
- PVD uses a heat source to evaporate the material of interest, which is then deposited onto a substrate.
- PVD enables creation of unique microstructure and morphology compared to pressed explosives.

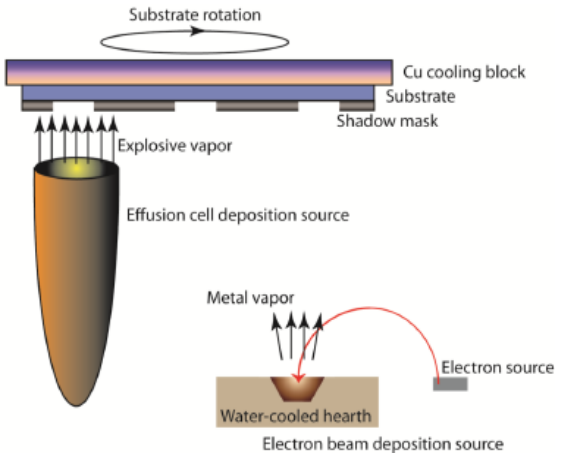

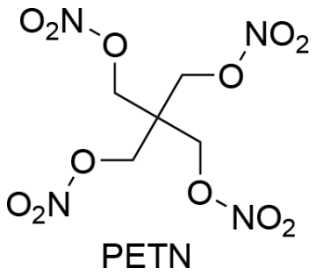

PETN

Custom high vacuum chamber for PVD of energetics (top) and schematic of deposition process (bottom) **[Knepper 2014].**

Typical explosive manufacturing methods do not allow controlled variation in microstructure

- Local variation in microstructure is common [Knepper 2011].

Comp A-5 Pellets [https://explosives.k2si.com].

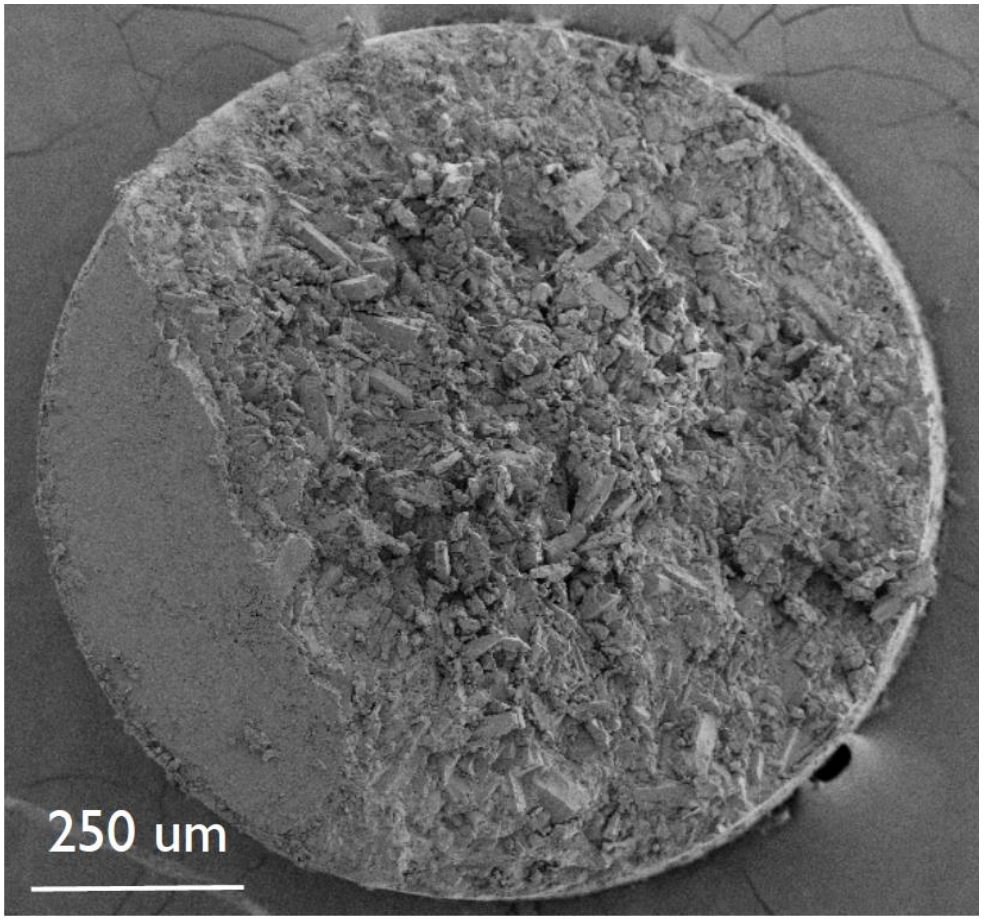

PETN Pellet Microstructure [Wixom 2008].

Morphology of PVD explosives can be controlled by deposition conditions

Increasing film Thickness

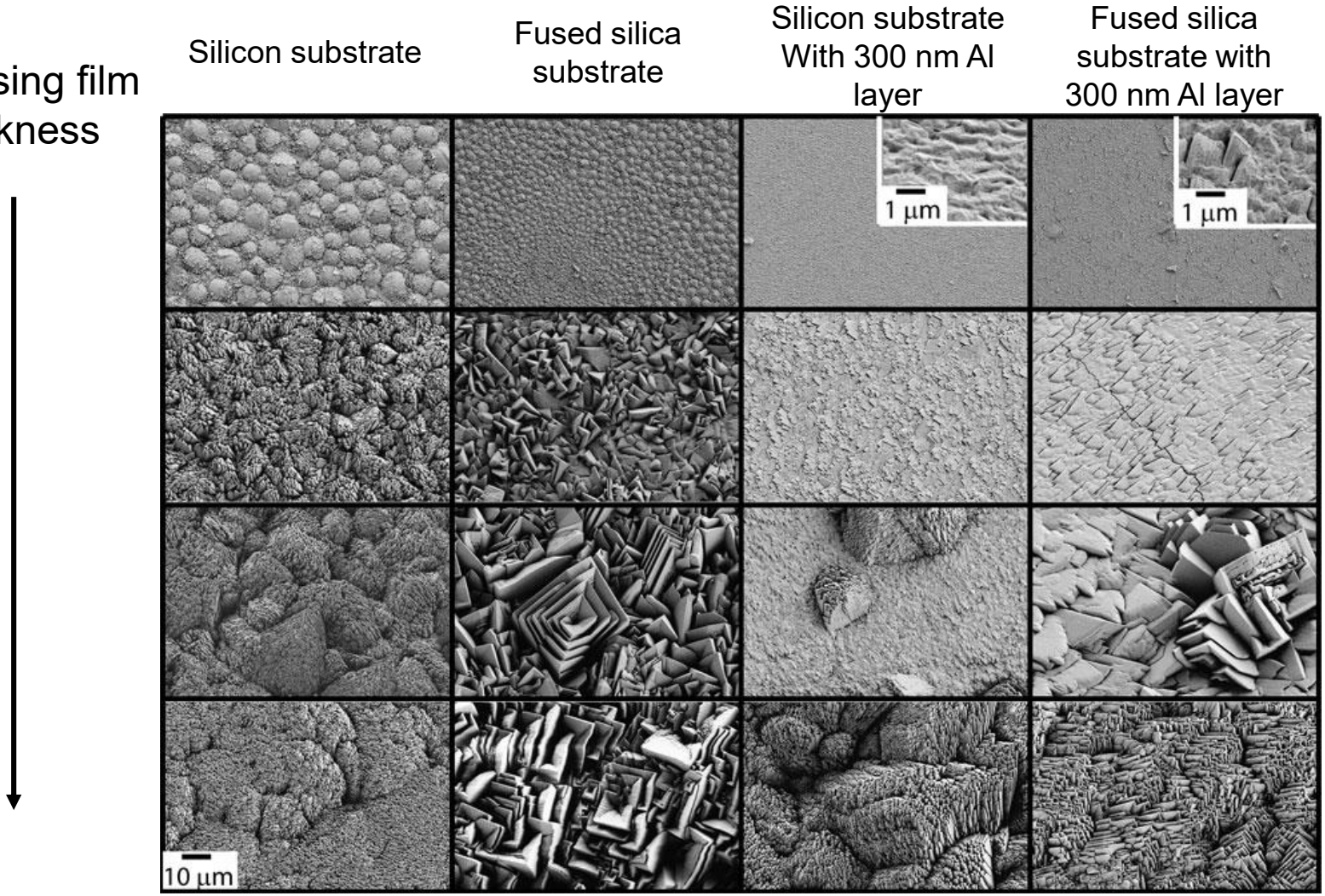

[Knepper 2011]

Microcracking can occur in high density pentaerythritol tetranitrate (PETN) films

- Films deposited onto substrates with higher surface energy:
  - Have higher density.
  - Have an increased detonation velocity [Forrest 2017, Knepper 2018].
- ***Effect of microcracks on detonation propagation in thin films is unknown.***

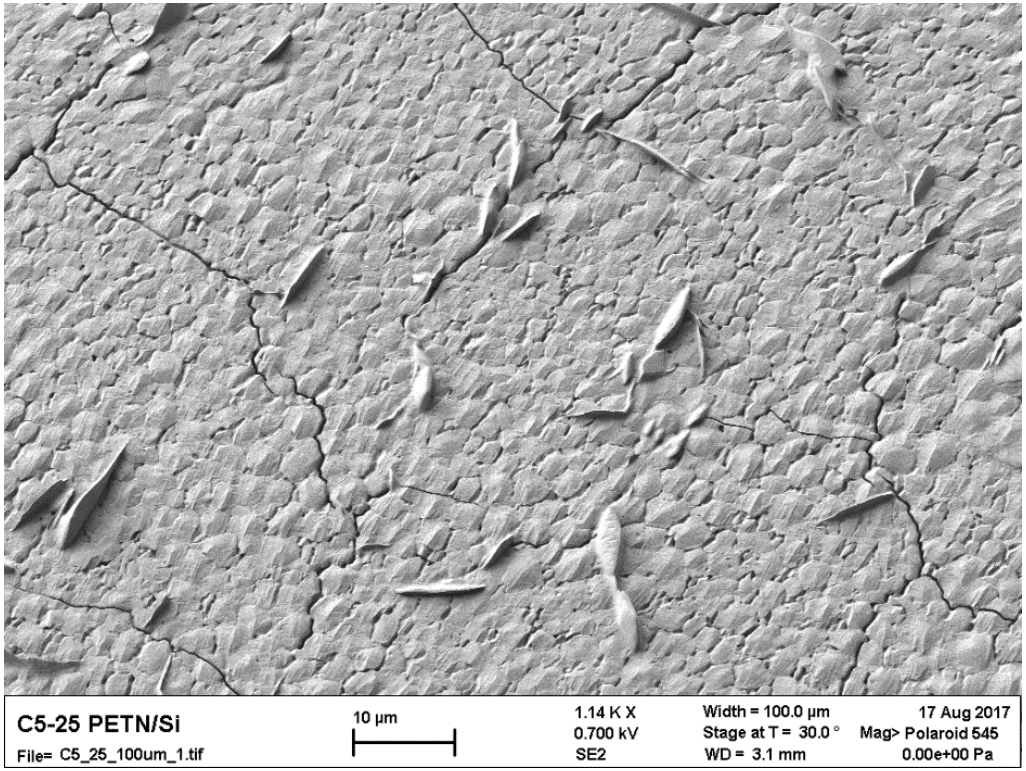

Scanning electron micrograph (SEM) of dense 10 µm thick PETN film on silicon substrate. Note cracking from residual thermal stress.

Detonation can fail at a length scale referred to as the critical dimension

- Typical critical dimension measurements are performed on cylinders.
- The critical thickness of a slab has been shown to roughly be equal to the critical diameter of a cylinder [Gibbs 1980, Campbell 1976, Dobratz 1985, Starkenberg 1998].
- PVD can create films close to their critical thickness [Knepper 2011, Tappan 2010, Tappan 2012].
  - Allows for study of films at near failure conditions.

Research here is to understand effect of microcracking on detonation failure of PETN

- Implementing artificial gaps between two films to determine size of gap detonation can propagate across.
- Using image processing techniques to extract position and velocity data.
- Modeling the PETN films with CTH.

PETN films were deposited onto polycarbonate substrates

- Unconfined PETN films were deposited at a thickness of:
  - 200 μm.
  - 400 μm.

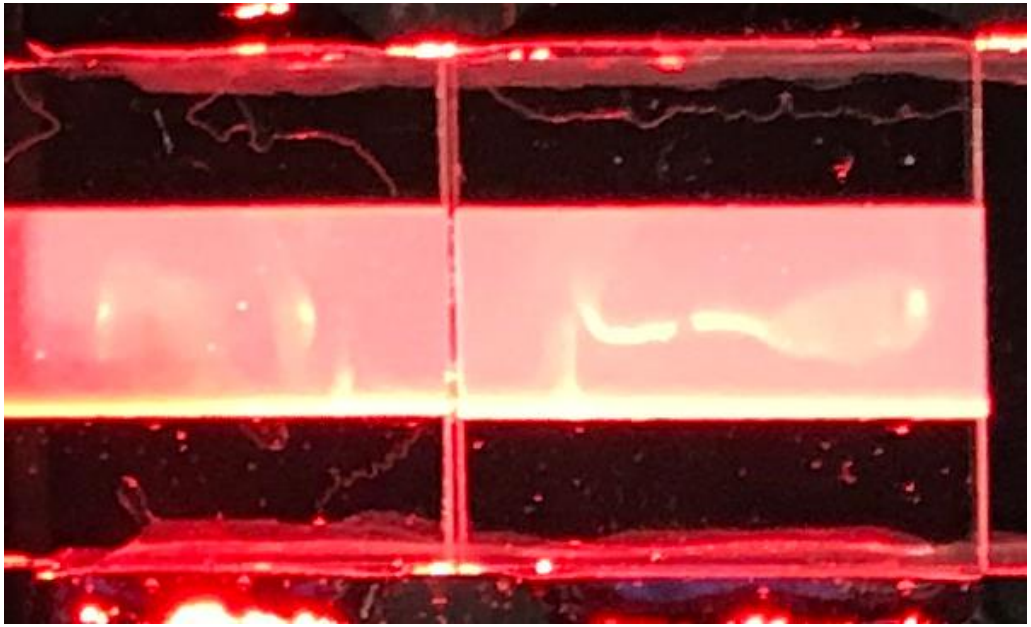

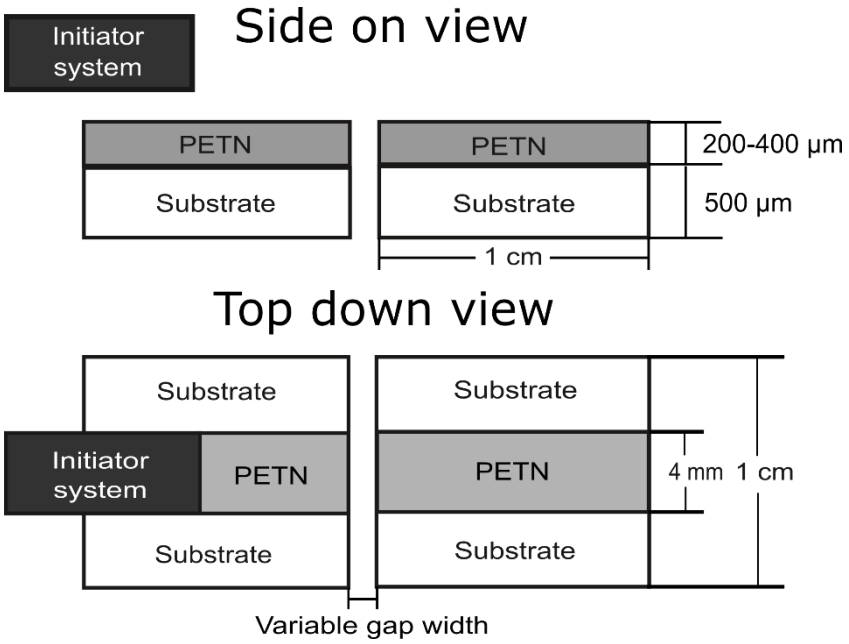

Top down view of PETN films with 95 μm gap.

PETN films with a 1 μm-thick aluminum (Al) confinement layer were deposited onto polycarbonate

- Two configurations were used:
  - An Al layer that remained in vacuum (bare aluminum, high surface energy).
  - An Al layer that was exposed to the atmosphere (oxidized Al, low surface energy).
- Confinement was used here to study the films at near failure conditions.
  - The effects of confinement were not explicitly explored.

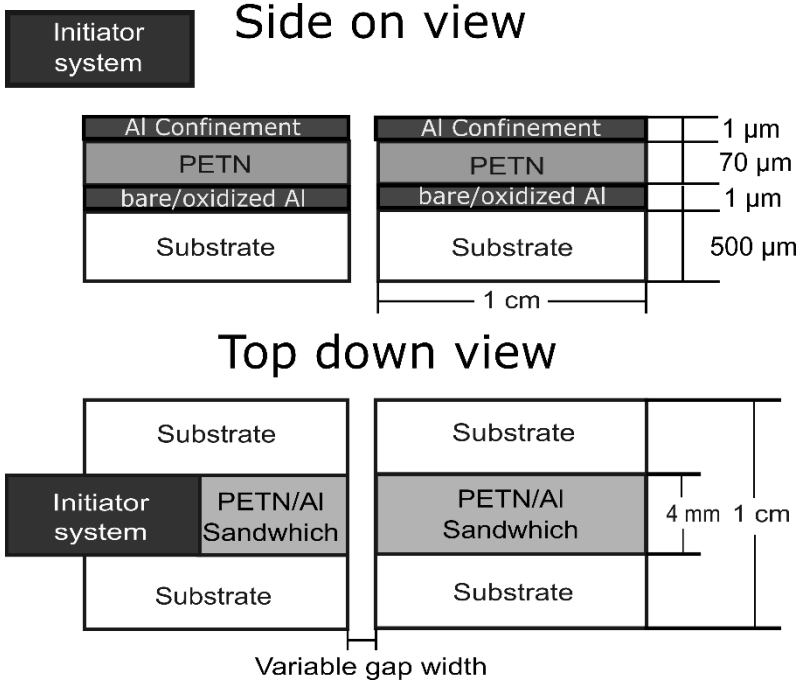

Refractive imaging visualizes shock in air

- Focused Shadowgraph visualizes the second derivative of the refractive index.
- Schlieren visualizes the first derivative of the refractive index.

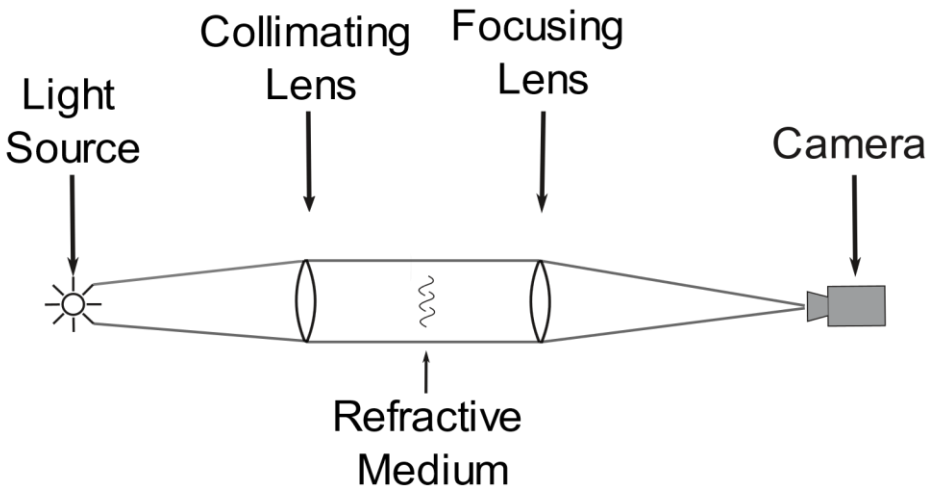

Focused shadowgraph system.

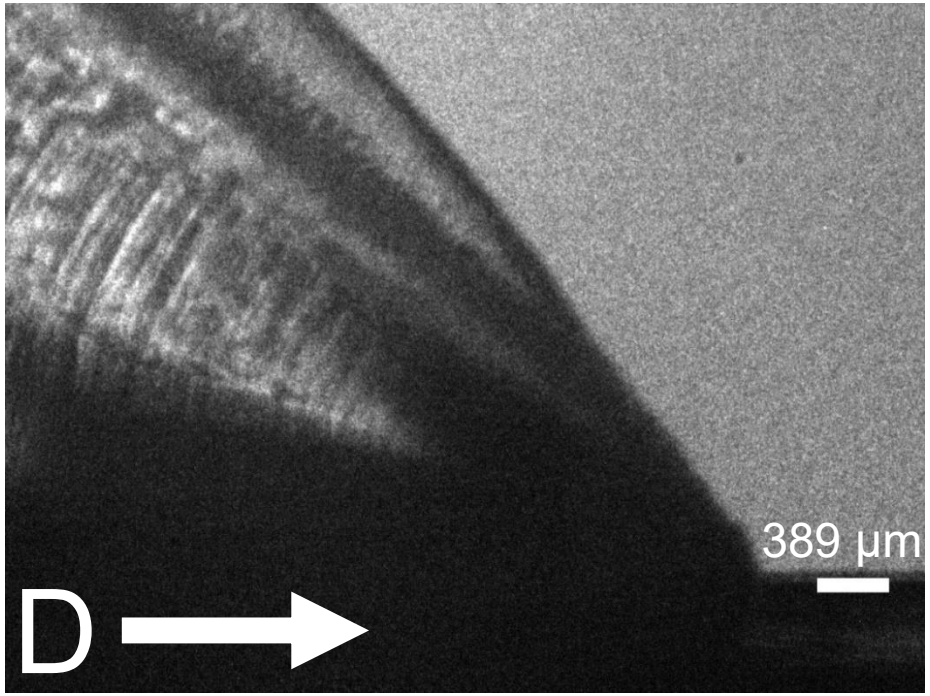

Schlieren image of a PVD PETN film detonating.

Imaging setup for measurement of the shock front

- Specialised Imaging SI-LUX 640 spoiled coherence laser used as light source for test.
- Camera was a Specialised Imaging SIMX-15.
  - Camera is capable of recording 15 full resolution images at a frame rate of up to 1 billion frames per second.
- Test was conducted in two series.
  - First test series used focused shadowgraph.
  - Second test series used schlieren.
- A 1 mm x 1 mm square calibration grid was used for converting pixel location to spatial location.

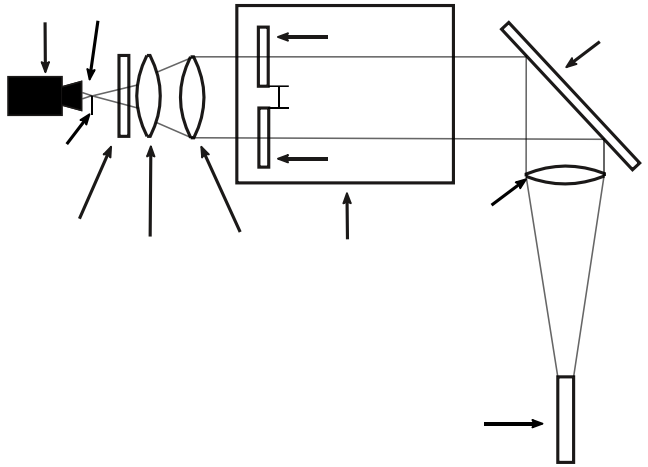

Test Series 2 schlieren with a horizontal field of view (FOV) of ~5.2 mm.

PETN Film fixture inside BoomBox.

Detonation tests to determine PETN failure

- Detonation tests include:
  - Continuous film test.
  - Gap test.
  - Infinite gap test.

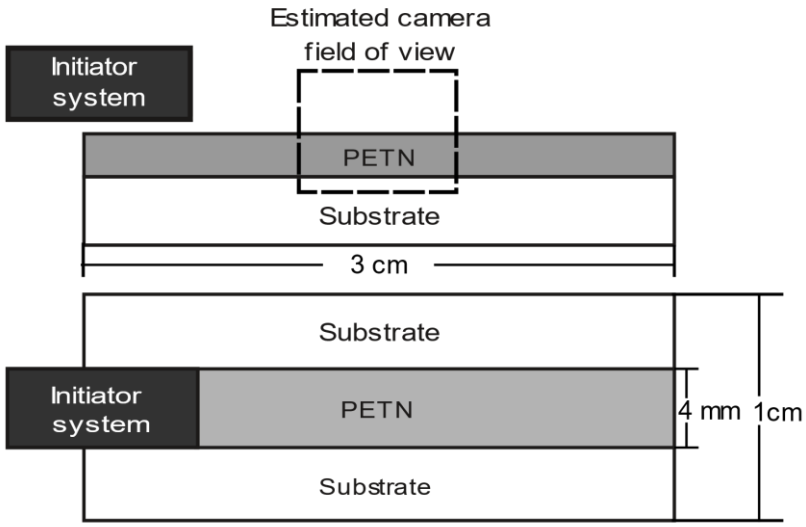

Continuous film test.

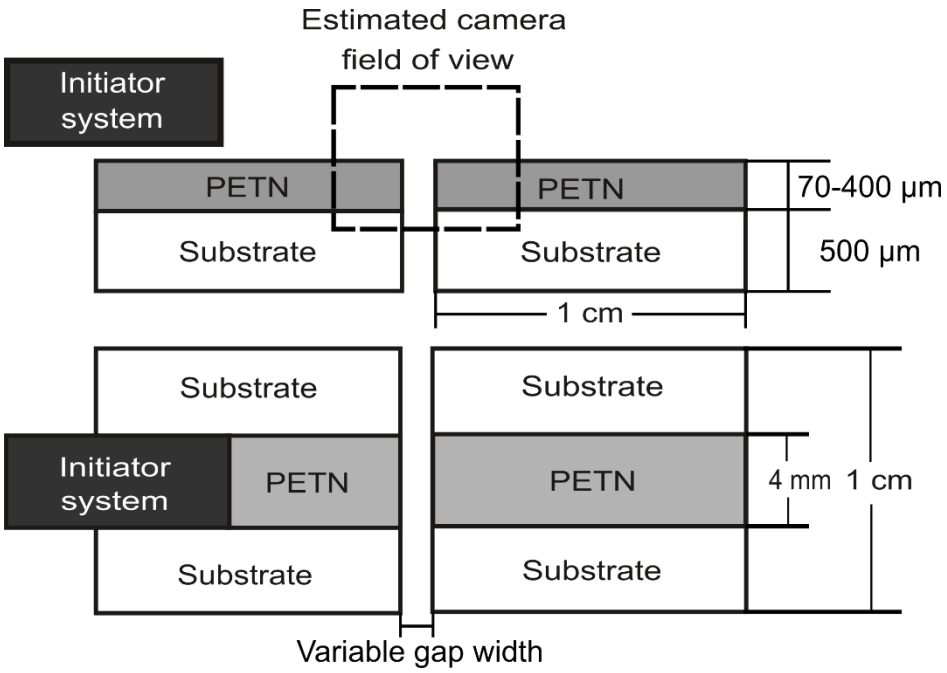

Gap test.

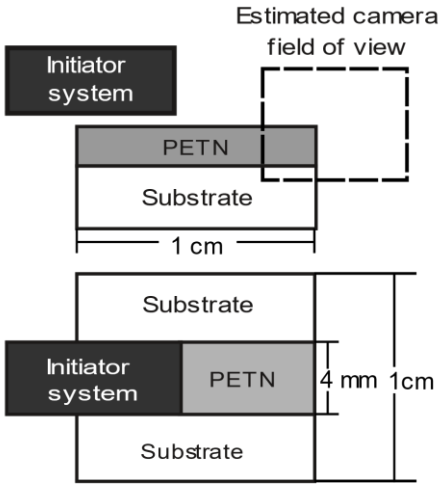

Infinite gap test.

70 μm-thick continuous film test

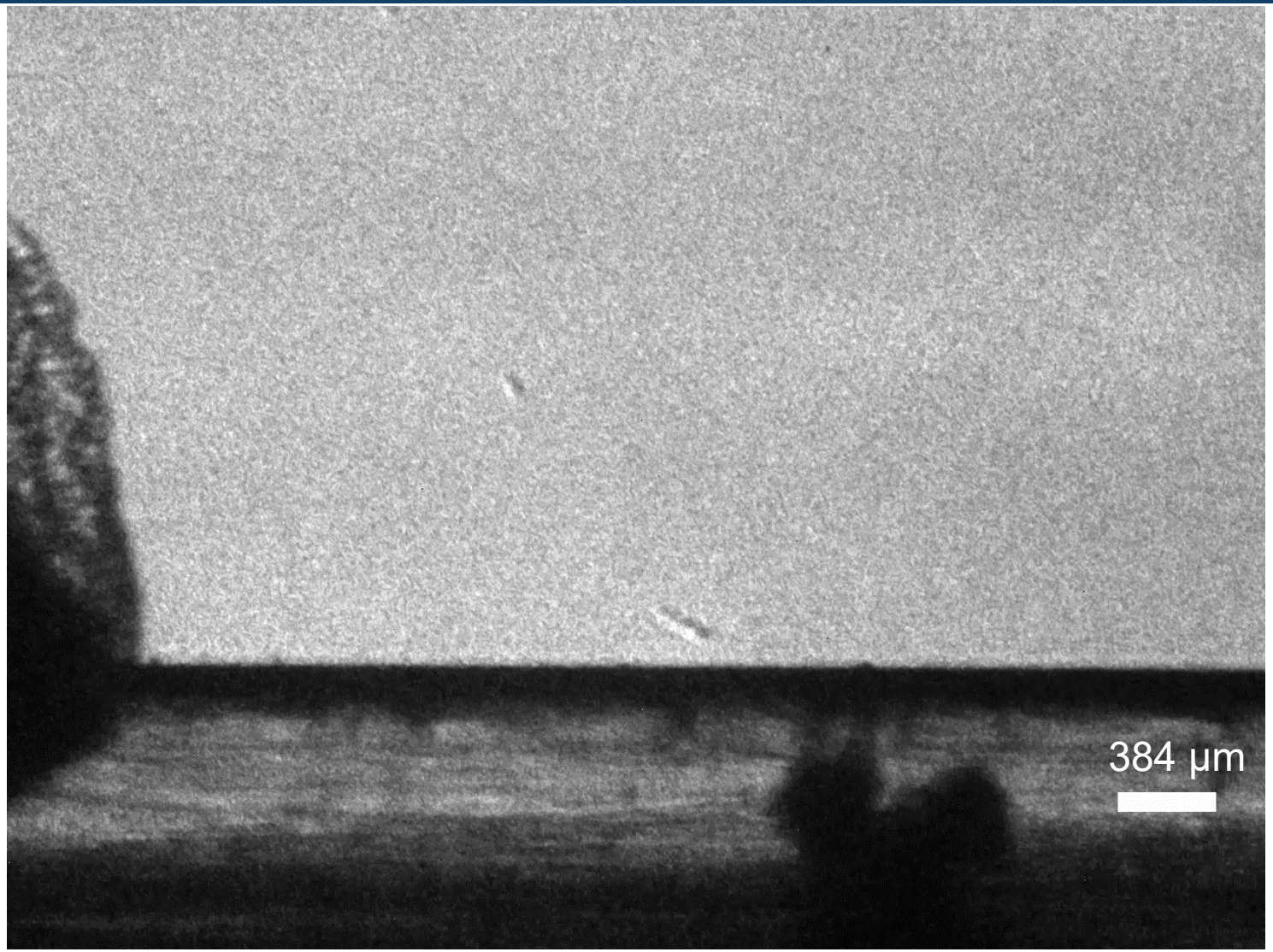

70 μm-thick continuous film test

- The 70 μm-thick aluminum confined PETN films display a rough shock front.
- The roughness could be caused by porosity within the microstructure.
- This effect is similar to Ramsay

  ,

  rough shock front caused by small discontinuities in explosives [Ramsay 1965].

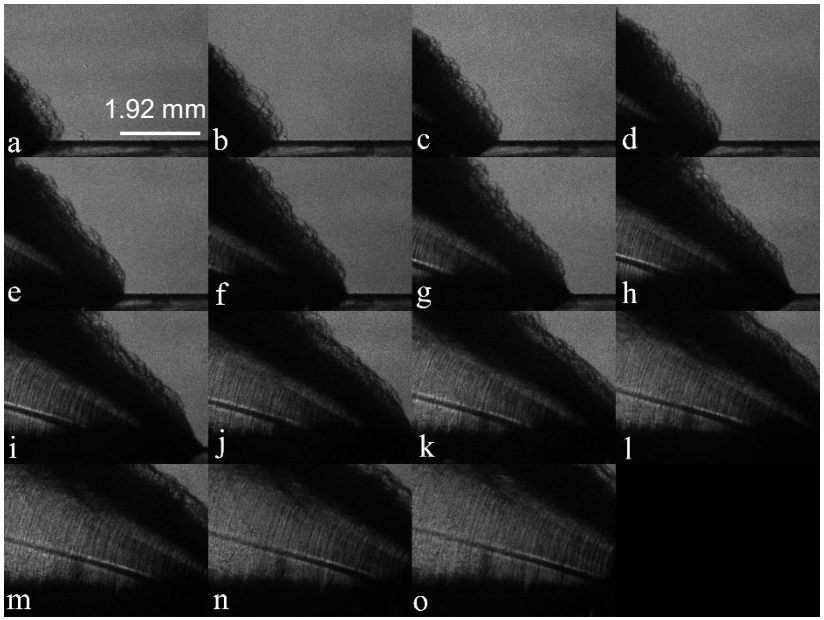

Schlieren detonation sequence of a 70 μm-thick Al confined film deposited on bare Al.

The shock produced by the 200 μm film is significantly more uniform than the 70 μm confined

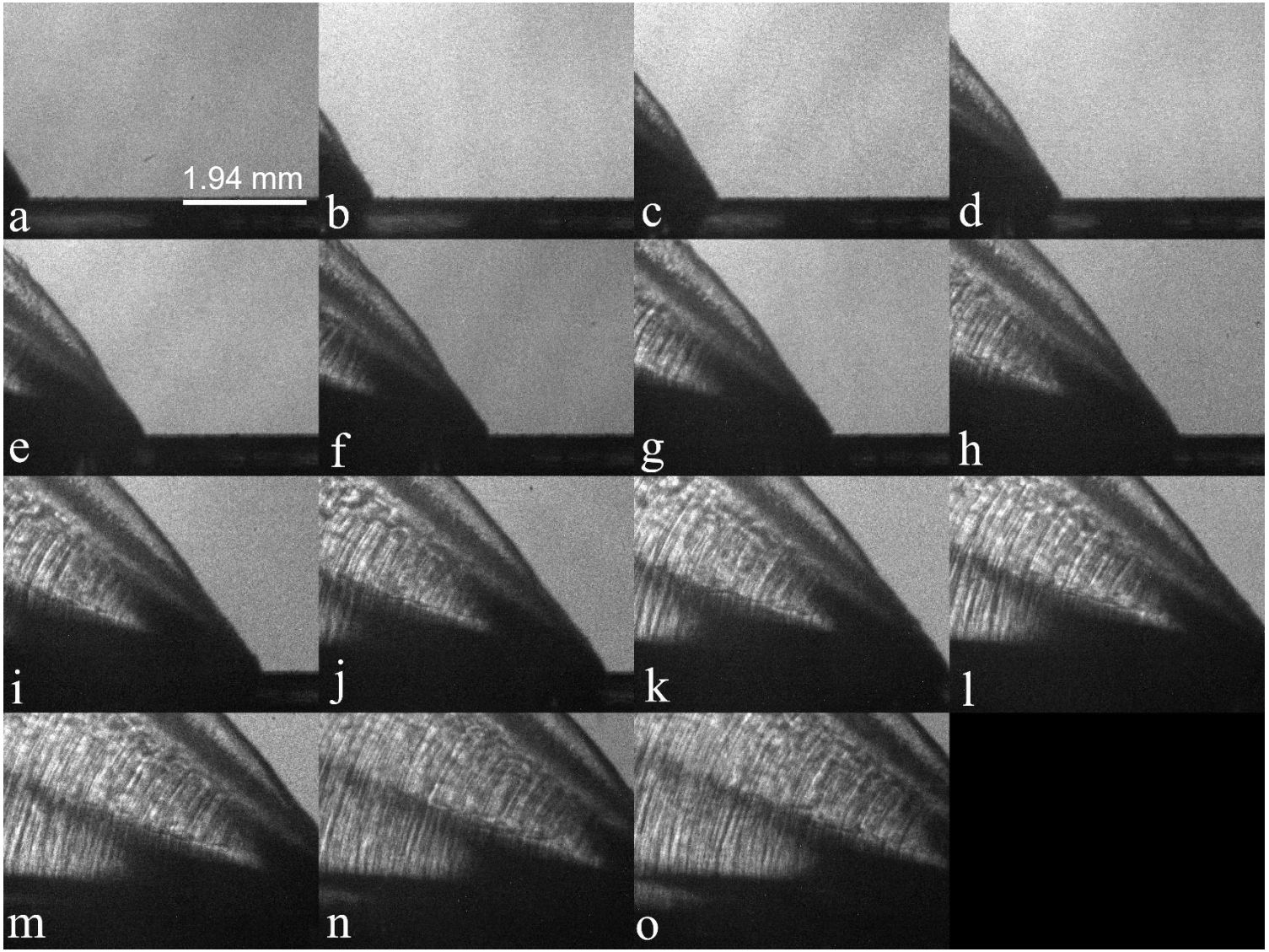

400 μm-thick film – Successful initiation across gap

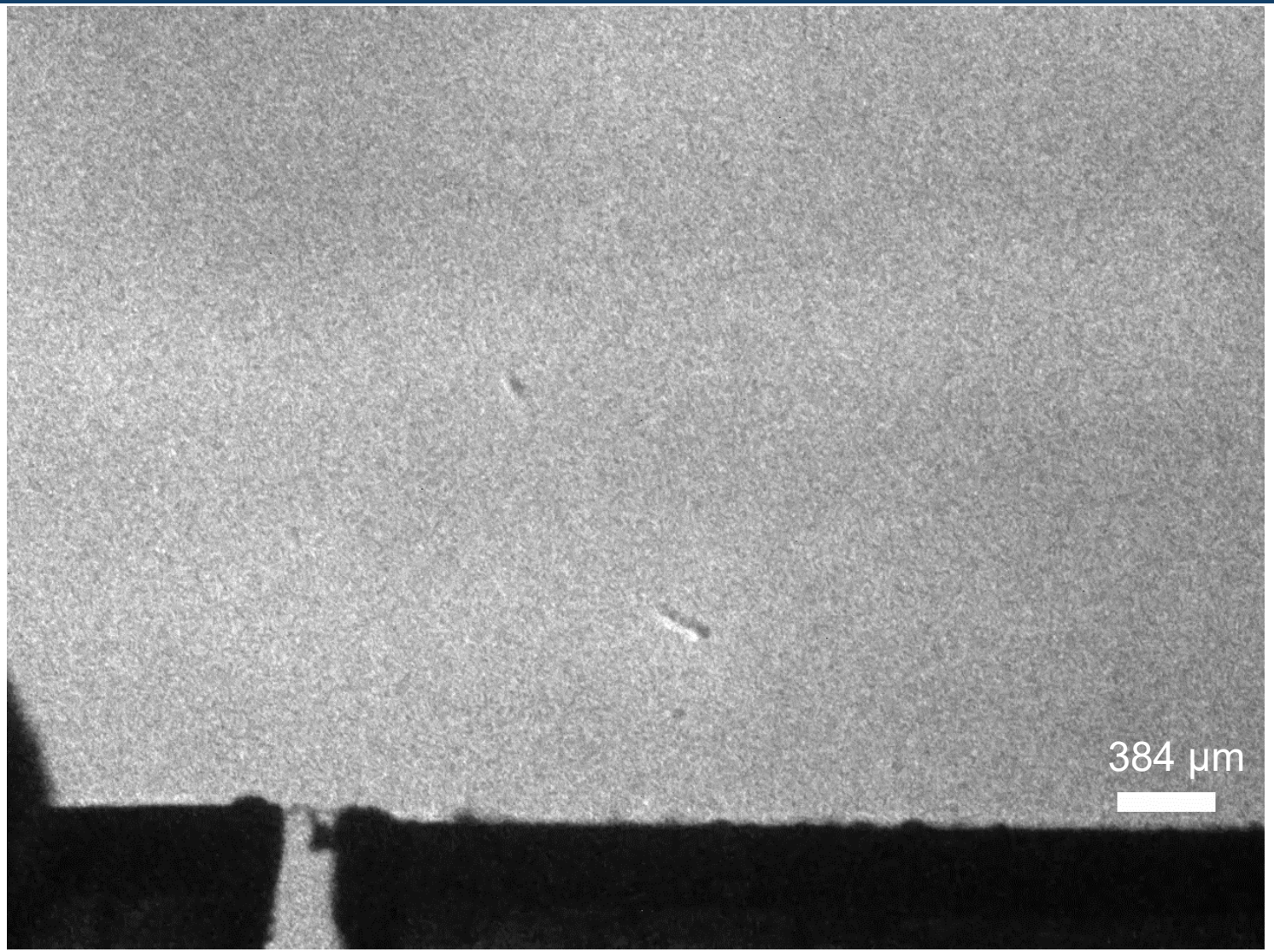

400 μm-thick film – Failure to initiate across gap

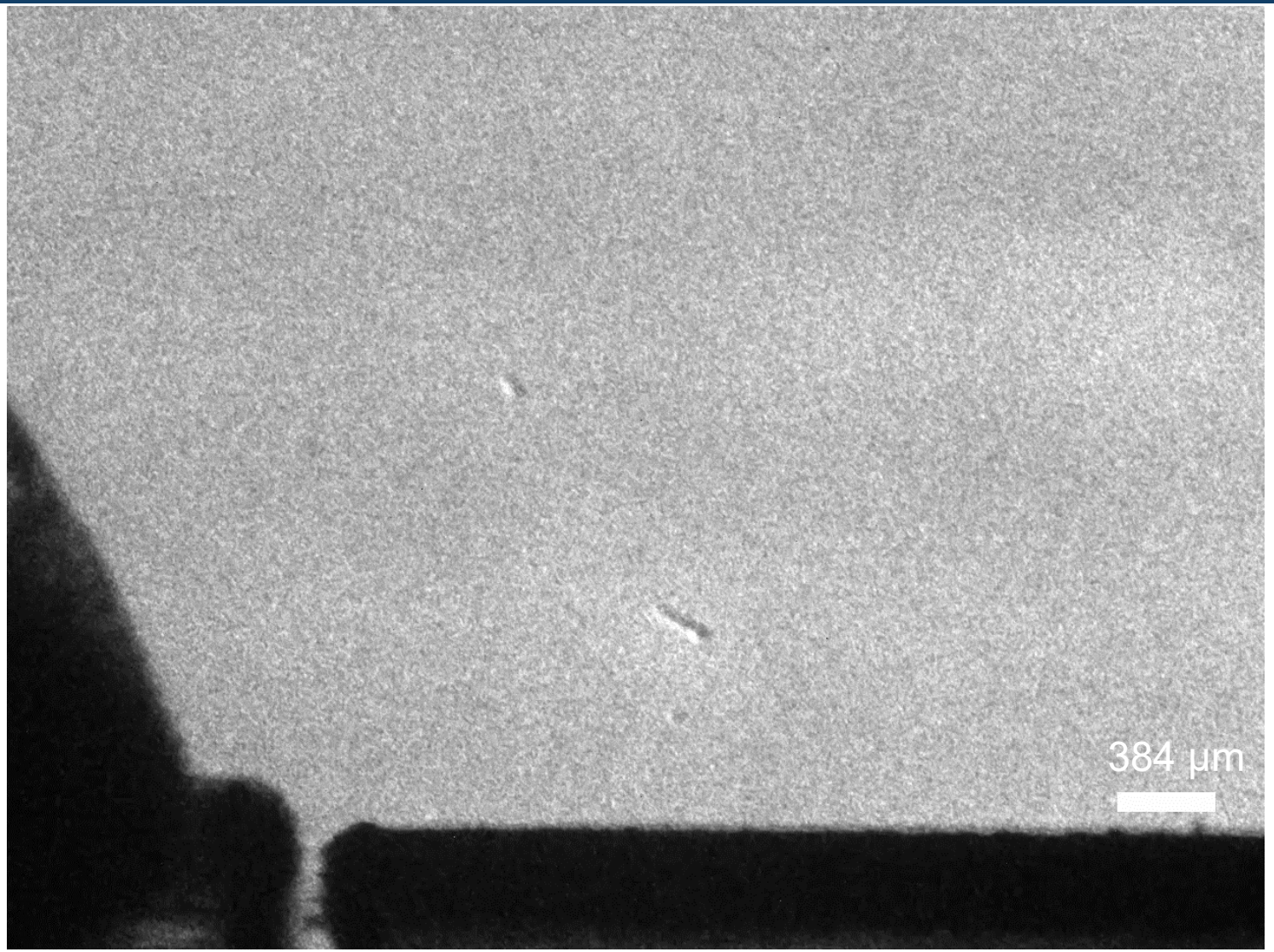

The post detonation substrates provide a supplementary indication of test results

- Detonation propagation was determined:
  - Successful if shock returned to steady-state shape.
  - Unsuccessful if shock front became circular.

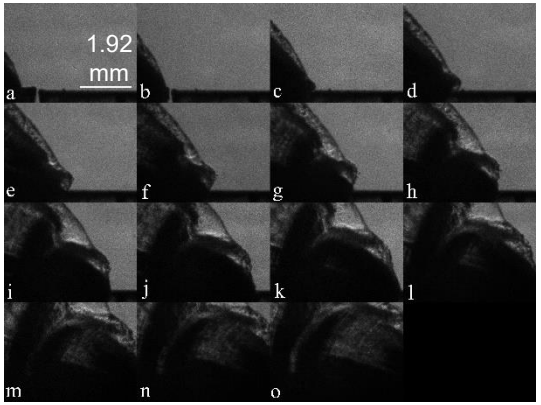

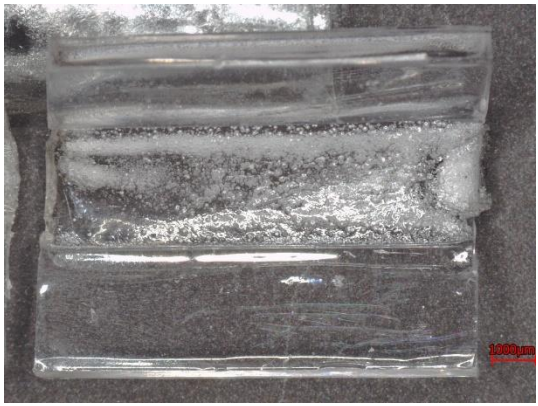

Successful detonation propagation.

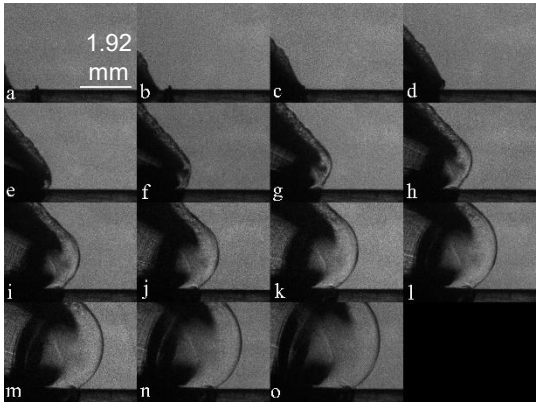

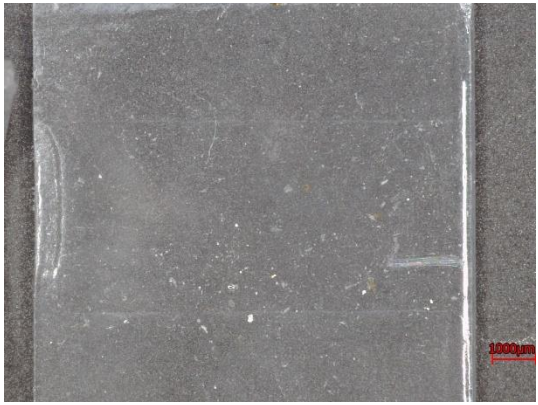

Failed detonation propagation.

Image processing to extract spatial data

- A custom-developed image processing routine was built to:
  - Highlight the shock wave.
  - Automatically extract and measure:
    - Shape.
    - Spatial coordinates.
    - Velocity.
- Canny filter [Canny 1986] alone was sufficient for extracting shock front in most images.
- Noisier images required use of additional image processing techniques.

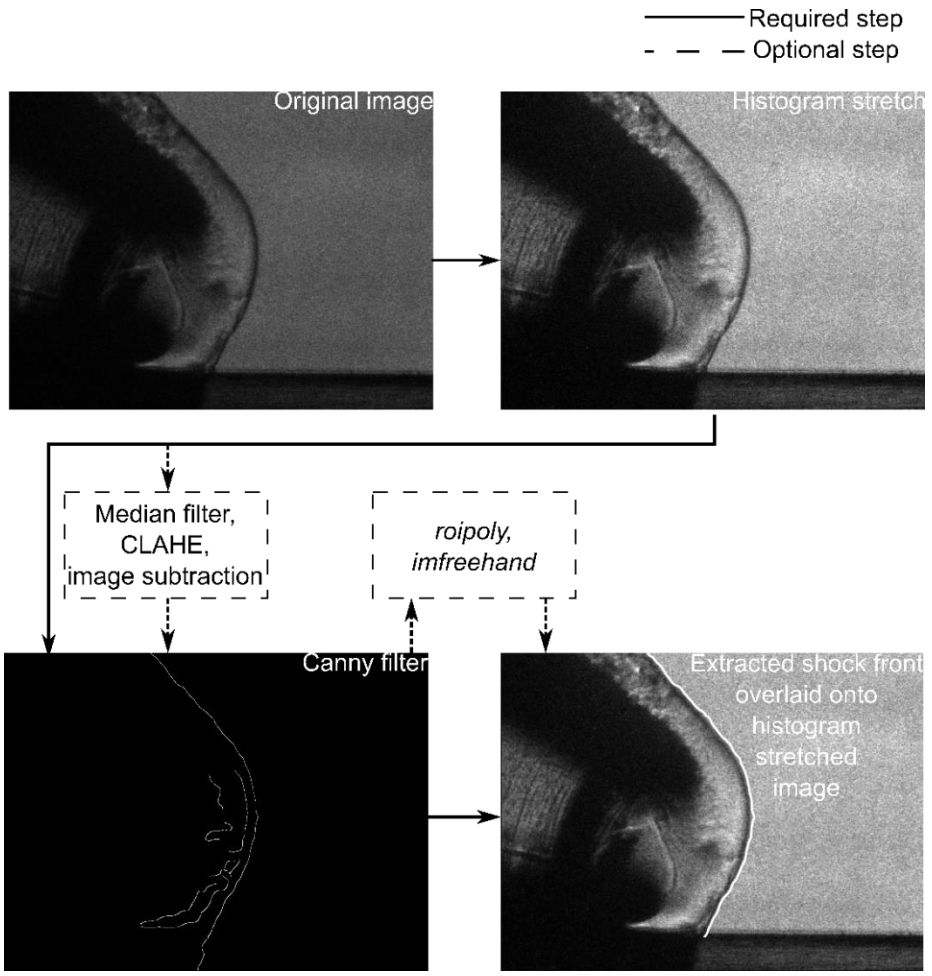

Normal velocity method for determining velocity of a pressure driven flow

- Velocity of shock wave is calculated from spatial data in successive frames [Chapra 2015].
- New method for automatically determining shock front velocity was developed that:
  - Calculates velocity in direction of dynamic pressure driven flow.

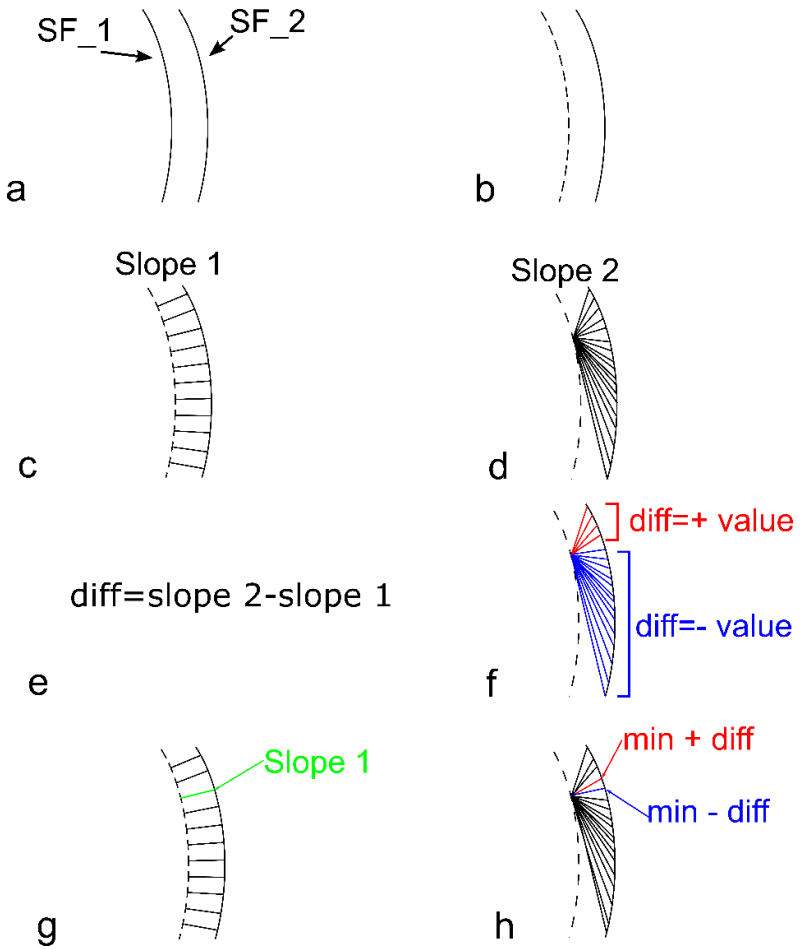

Normal velocity plots were made to visualize velocity of the shock front

- The plots are color coded to specify velocity.
- Black vectors are rejected due to an uncertainty in slope matching > ± 50 m/s.

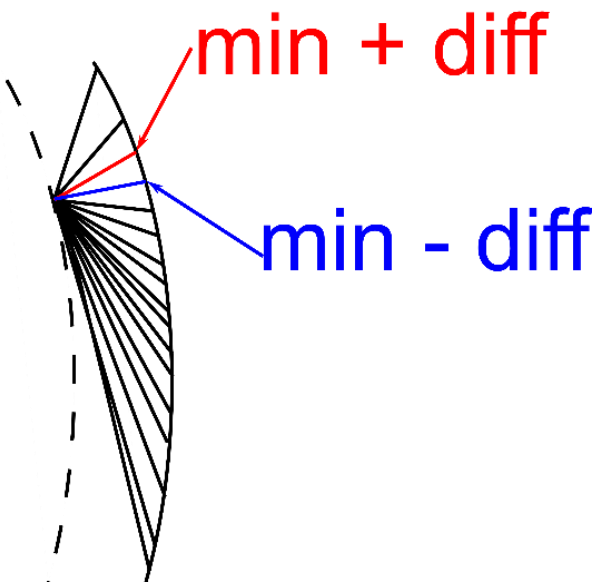

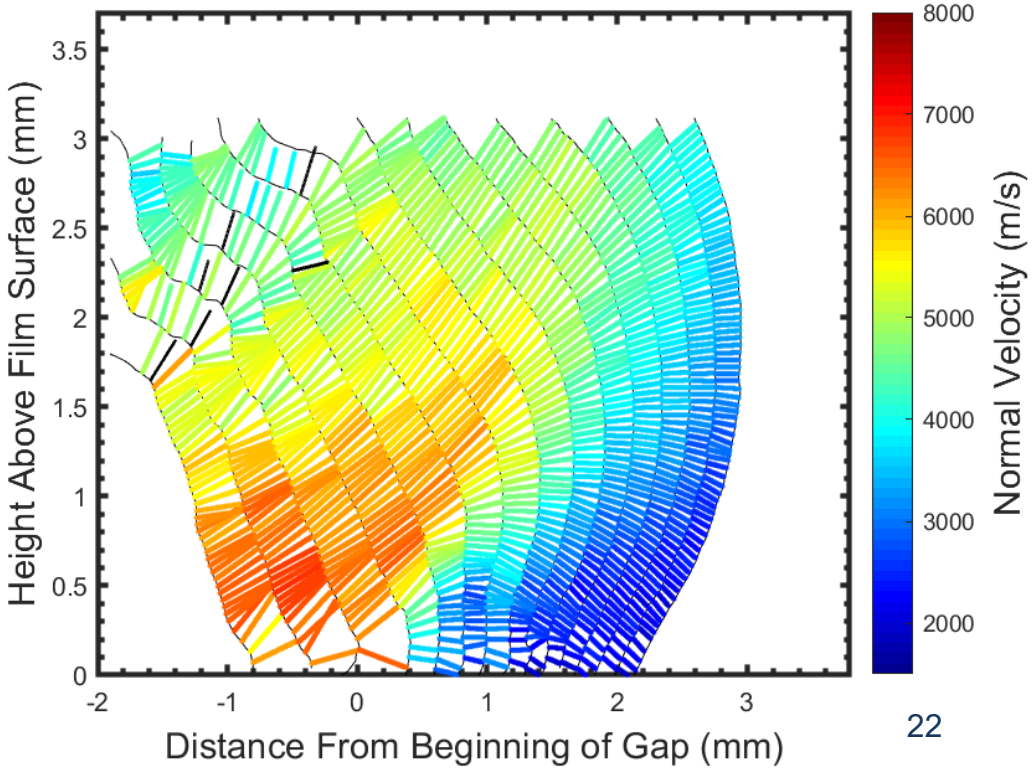

Continuous film test with transient shock

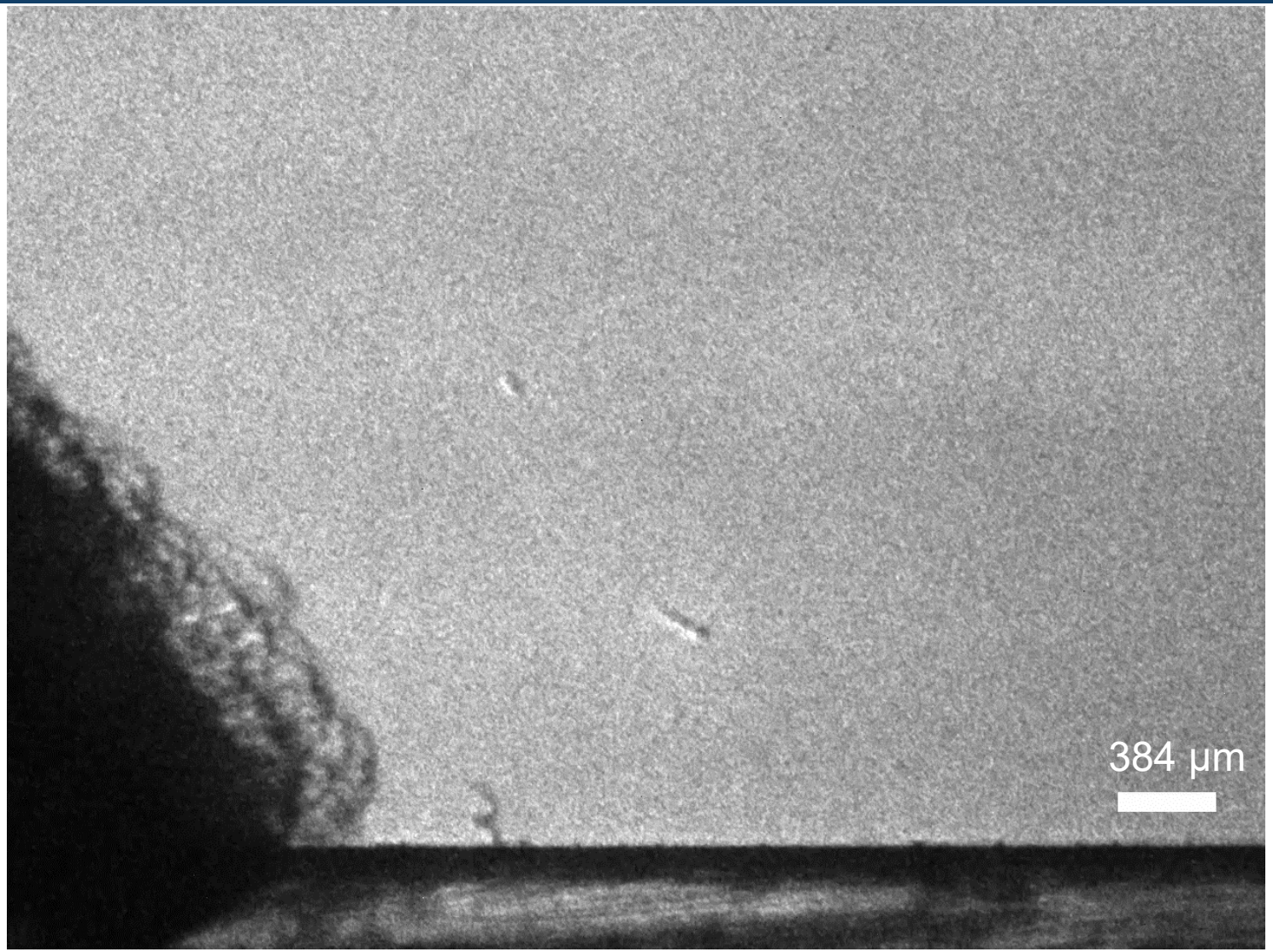

Transient velocity is an indicator of when detonation reached steady-state

- The velocity of the shock front increases as the shock front reaches steady-state.
- The height of the steady-state velocity was recorded for each of the tests at:
  - The vertical plane representing the beginning of the gap (0 plane).

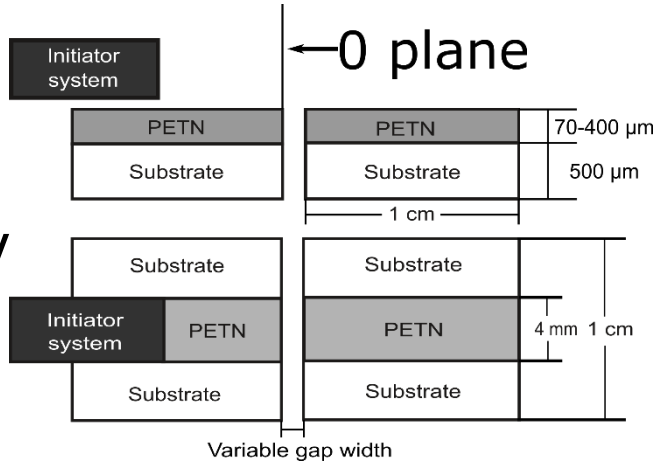

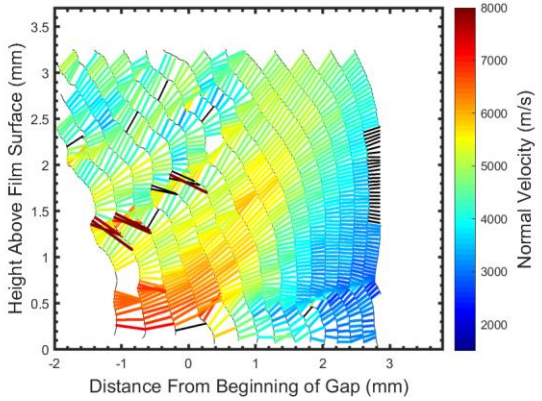

70 μm-thick film deposited on oxidized aluminum.
1 mm above the film surface.

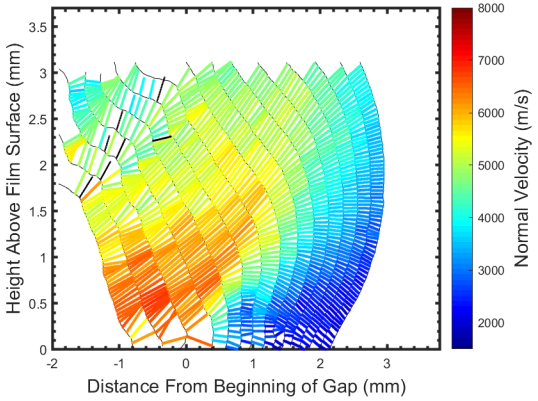

70 μm-thick film deposited on bare aluminum.
1.5 mm above the film surface.

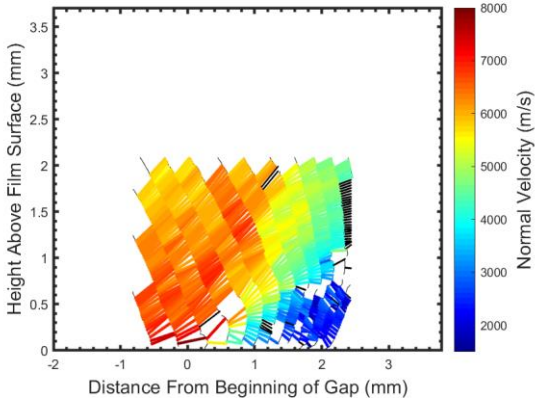

200 μm-thick film.
≥ . v

Successful initiation

- The distance the shock front traveled before returning to its steady-state wave shape for a:
  - 200 μm film with a 25 μm-gap-width was about 875 μm.
  - 400 μm film with a 220 μm-gap-width was about 1700 μm.

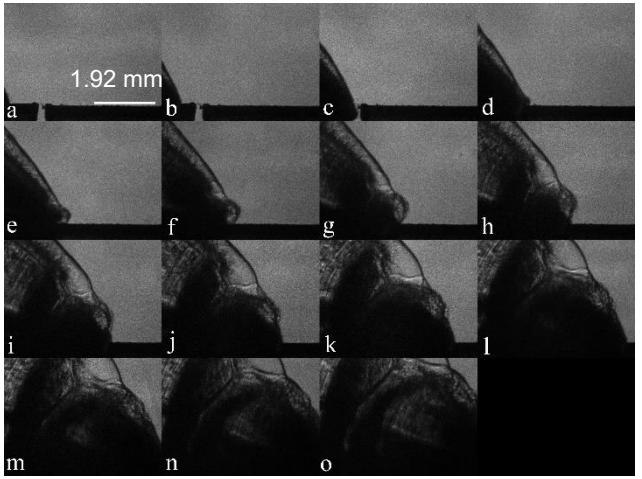

Schlieren images of a 400 μm-thick film gap test.

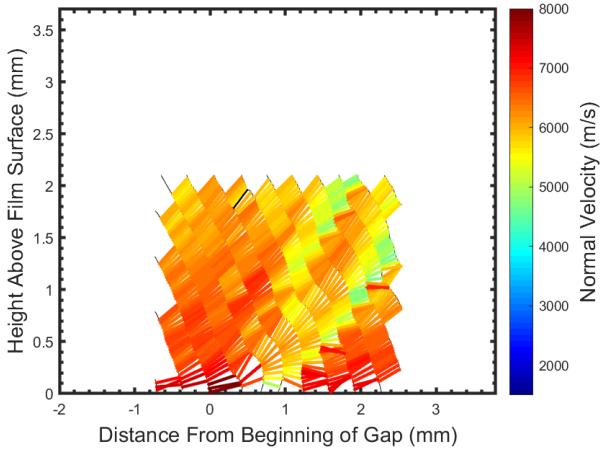

200 μm film velocity plot.

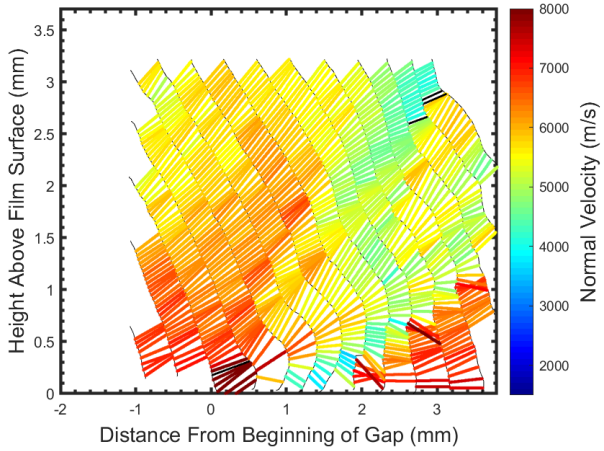

400 μm film velocity plot.

Critical gap width is the largest gap width for reliable initiation

- Neither of the 70 μm-thick Al confined films propagated across an abutment gap.
  - Close to critical thickness of Al confined films (55 μm) [Knepper 2018].
- The 200 and 400 μm-thick films both had detonations occur in gaps larger than the critical gap width.
  - May be due to roughness at edge of films.
  - No detonation failed below critical thickness.

Film Thickness (μm)	Critical Gap Width (μm)	Substrate Material
70	0	Oxidized aluminum
70	0	Bare aluminum
200	80	Polycarbonate
400	180	Polycarbonate

200 μm-thick film infinite gap test

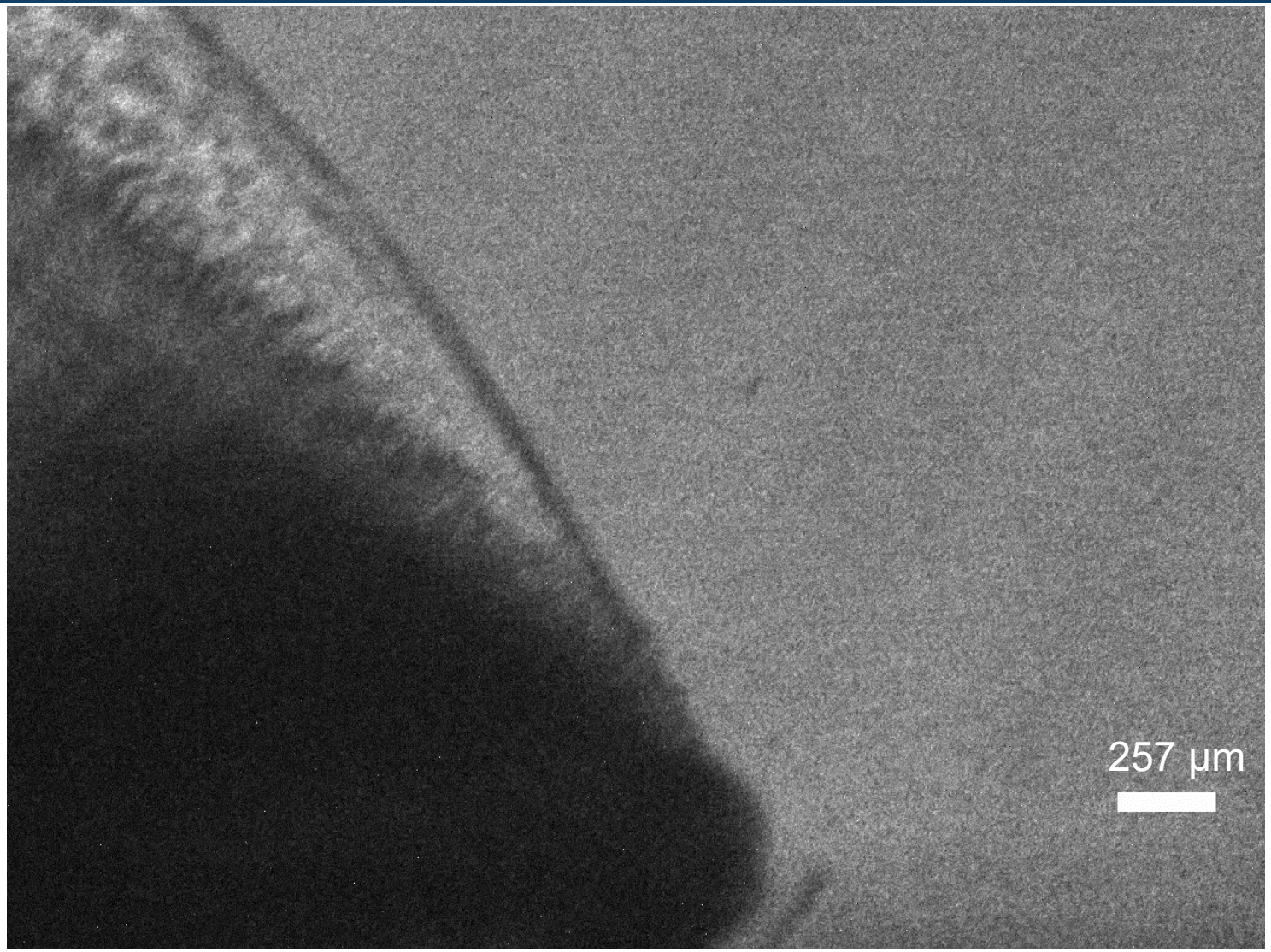

The velocity of the shock front within the gap is determined with the infinite gap test

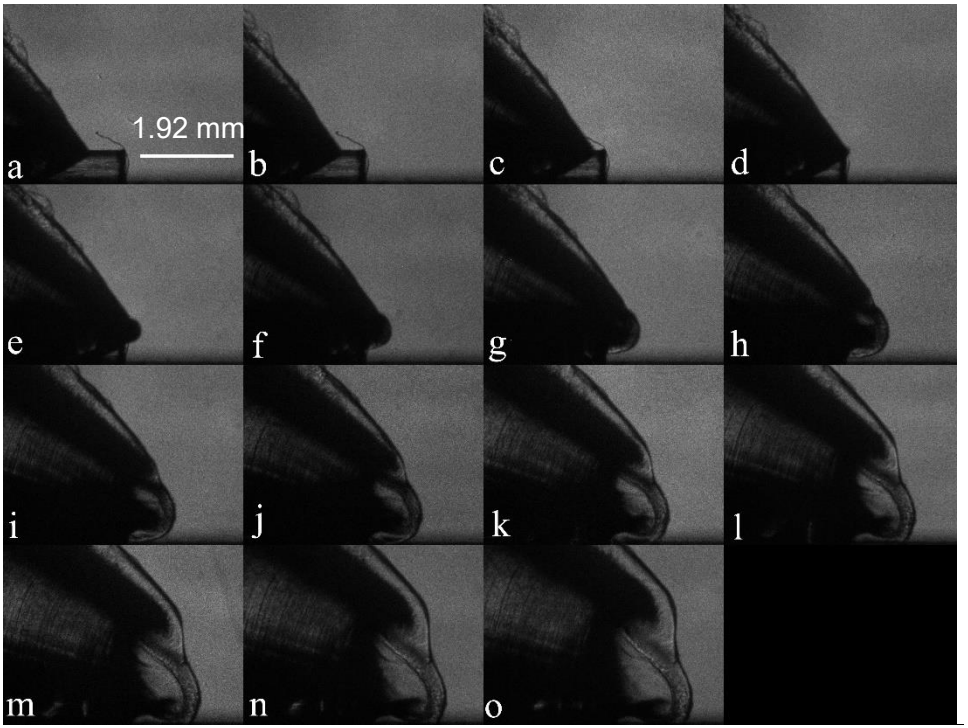

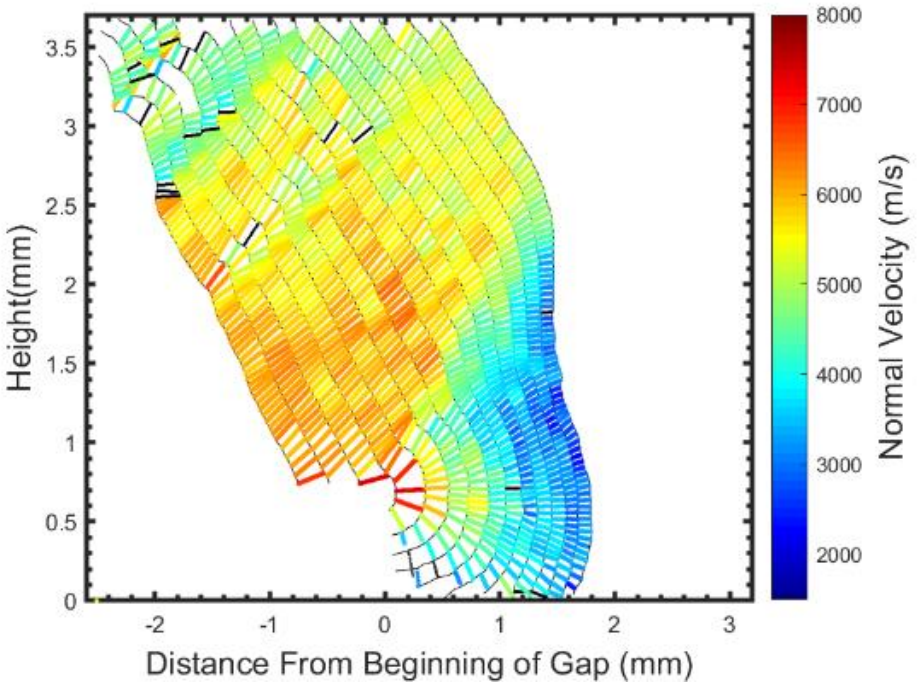

Hydrocodes numerically solve conservation equations

- CTH is an Eulerian hydrocode developed by Sandia National Labs.
- Hydrocodes typically use composite models to describe an energetic material.
- The composite models relate two equations of state (EOS) that describe:
  - The unreacted material properties.
  - The reaction product properties.
- The composite model relates the EOSs using an empirically derived burn rate.

2-Dimensional CTH model of PETN films

- The model consisted of:
  - PETN initiator (Jones Wilkins Lee (JWL) EOS).
  - PETN films with history variable reactive burn (HVRB) composite model:
    - Mie Grüneisen solid EOS.
    - Sesame tabular reaction product EOS.

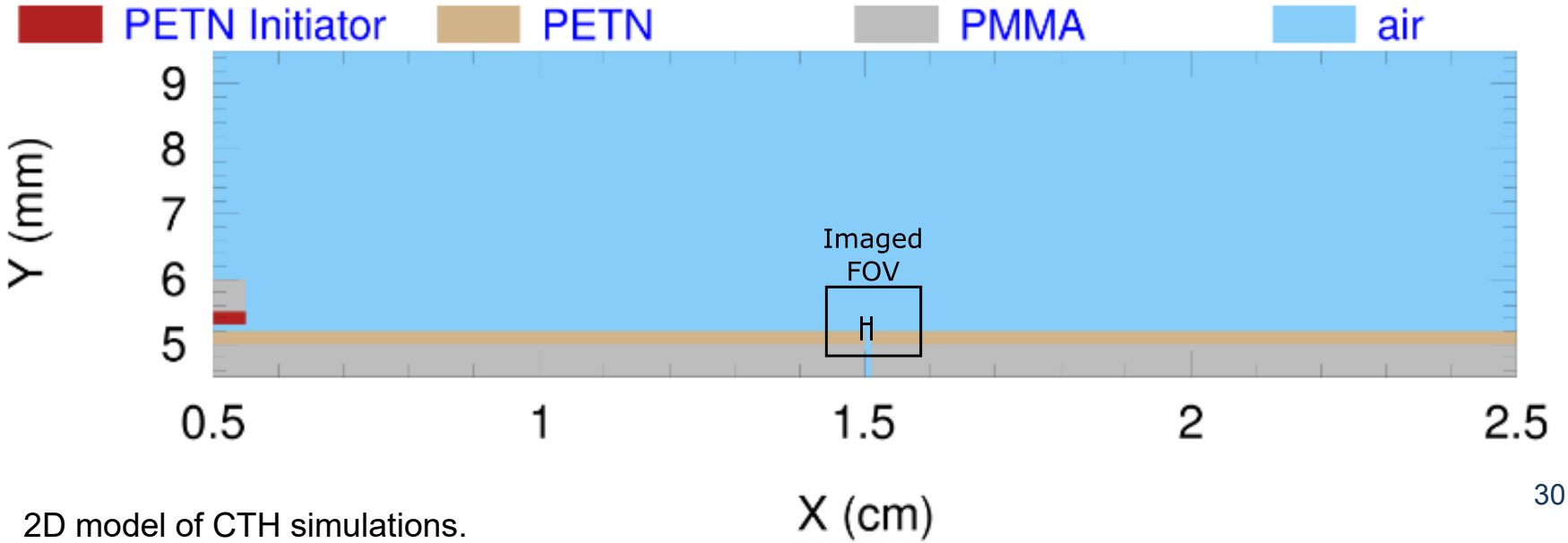

2D model of CTH simulations.

CTH density output

Derivative of the density field yields schlieren

- Schlieren images are the first derivative of the refractive index field.
- Density, ρ, is linearly proportional to the refractive index, *n*.

$$\rho = \frac{n-1}{k}$$

k is the Gladstone-Dale Coefficient.

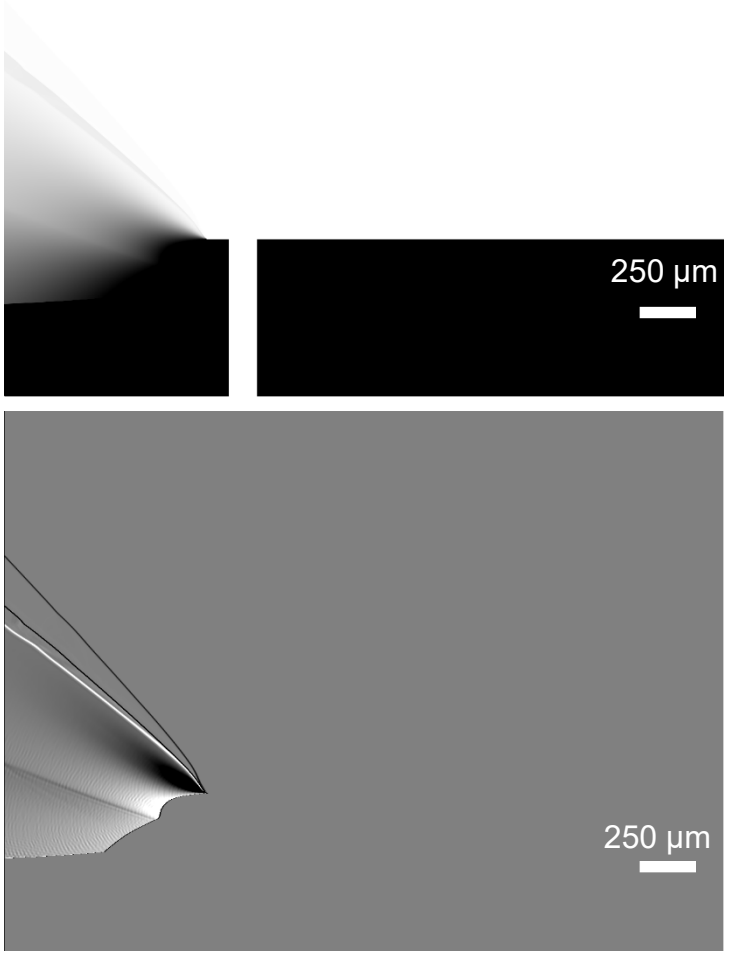

CTH continuous film test

- The detonation velocity was calculated for each of the continuous film tests.
- The calculation of the detonation velocity was performed by:
  - Manually clicking on the shock front along the edge of the film on successive frames.
- A total of 9 centered difference velocity calculations were performed for each test.
- The mean and standard deviation of the calculations is reported below.

Expt. / CTH	Film Thickness (μm)	Detonation Velocity (m/s)	Substrate Material
Expt.	70	7450 ± 116	Oxidized aluminum
Expt.	70	7910 ± 53	Bare aluminum
Expt.	200	7651 ± 197	Polycarbonate
CTH	200	7319 ± 88	PMMA

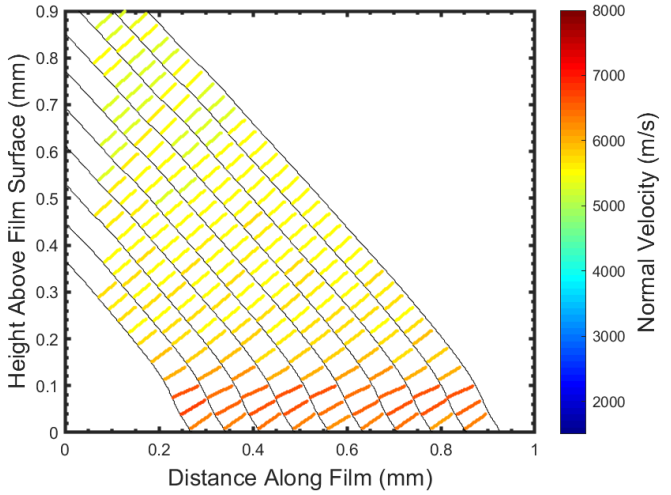

Continuous film CTH test.

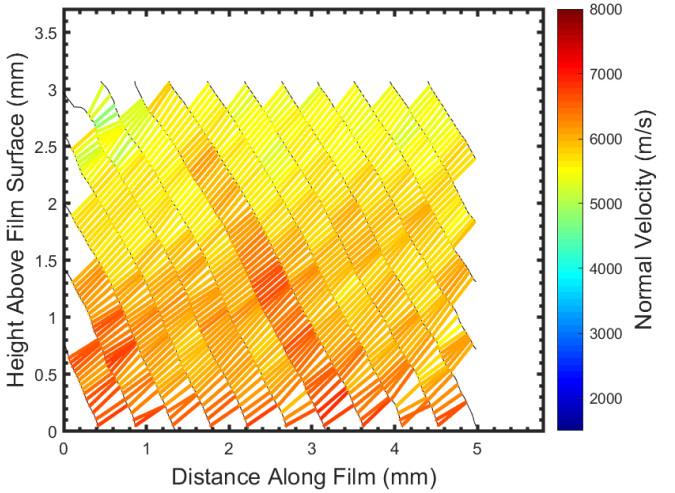

Continuous film experimental test.

200 µm-thick films were modeled with CTH

- The models were calibrated to initiate at a 200 µm-thickness.
  - HVRB
    - Calibration constants [Starkenberg 1998]
      - Pr=1e10
      - Z=3.9
      - PI=4e10 Threshold pressure for reaction
  - Mie Grüneisen
    - rho=1.5 Density of PETN
  - Tuned until critical thickness was roughly that of experiment.
- The critical gap width of the CTH tests was found to be 125 µm.

Expt./ CTH	Film Thickness (µm)	Critical Gap Width (µm)	Substrate Material
Expt.	70	0	Oxidized aluminum
Expt.	70	0	Bare aluminum
Expt.	200	80	Polycarbonate
CTH	200	125	PMMA
Expt.	400	180	Polycarbonate

Successful initiation video 125 μm gap computer generated schlieren (CGS)

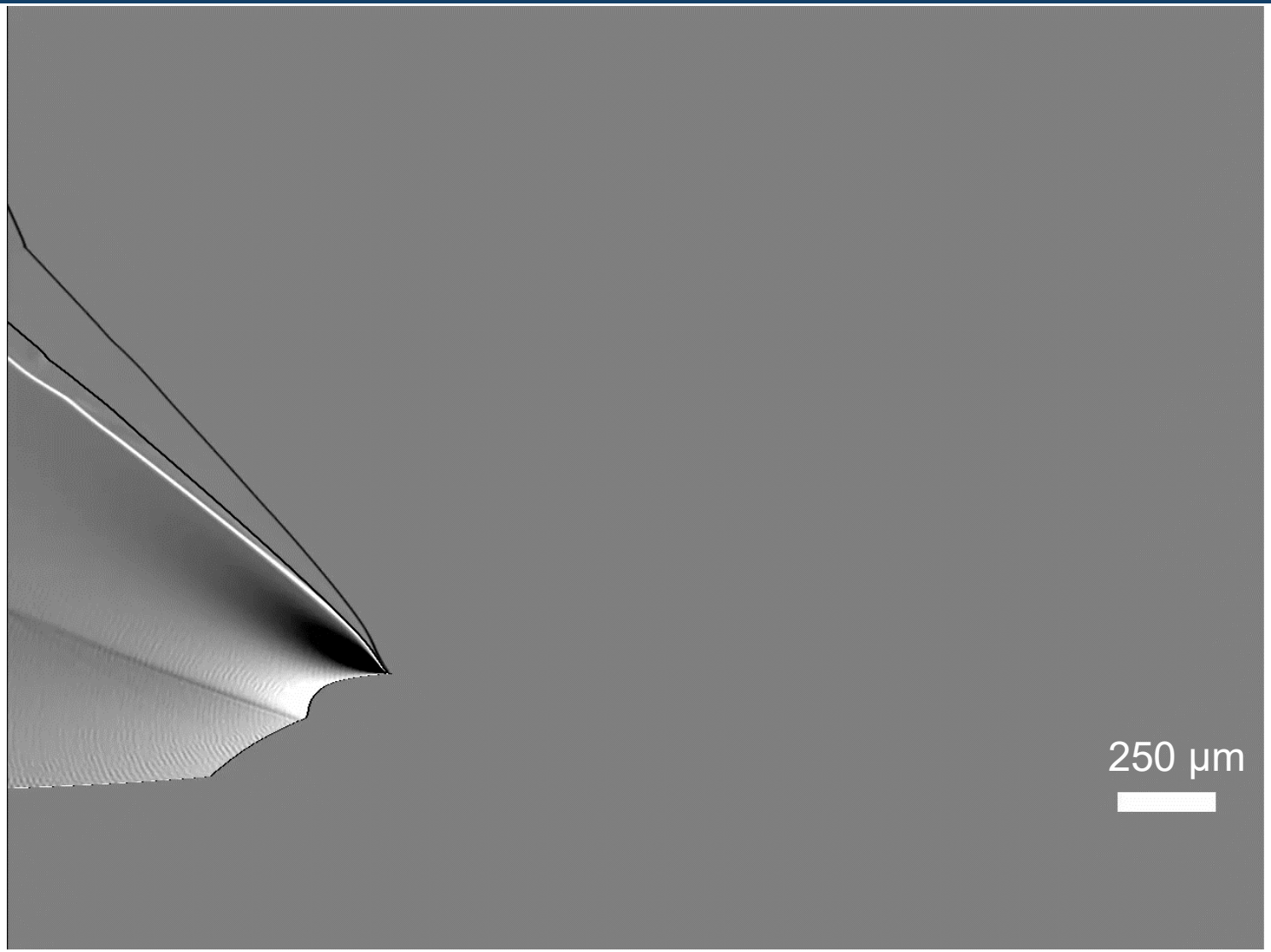

CTH successful initiation comparison

- In the experiments the outward protrusion in the shock front after the detonation passes the gap is now in the shape of a notch.
- The second film initiates almost immediately without allowing the air shock from the first film to create an outward protrusion:
  - Due to a lower run distance in the CTH films.

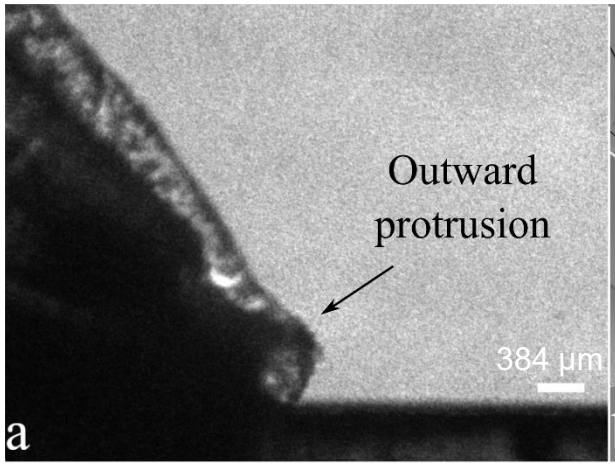

Experimental image.

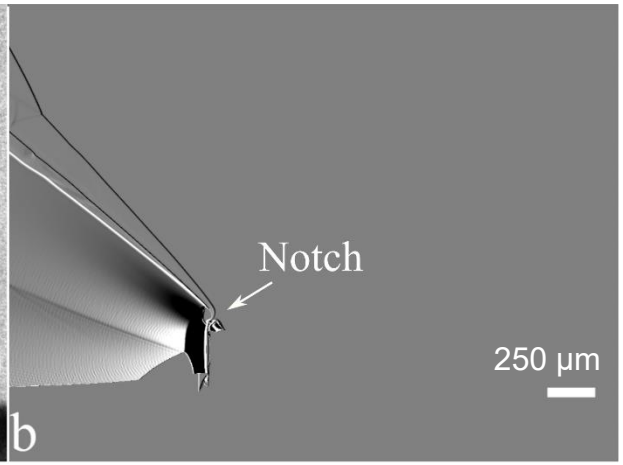

CGS image.

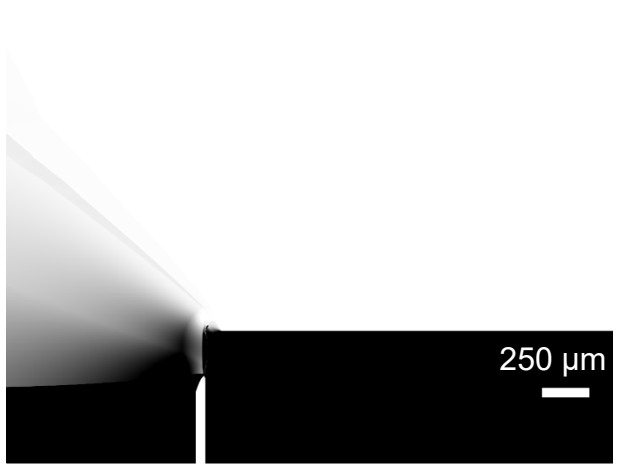

CTH density image.

There is significantly less disruption to the shock front in CTH

- The disruption in the shock front returns to steady-state rapidly.
- The distance to a steady-state wave shape is significantly shorter than in the experiments.

Expt./ CTH	Film Thickness (µm)	Gap Width (µm)	Distance to steady state wave shape
Experimental	200	25	875 µm
CTH	200	100	200 µm

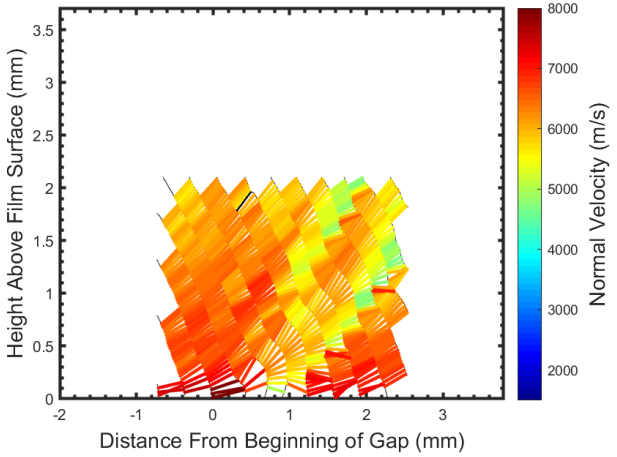

200 µm-thick film experimental gap test with a 25 µm-gap-width.

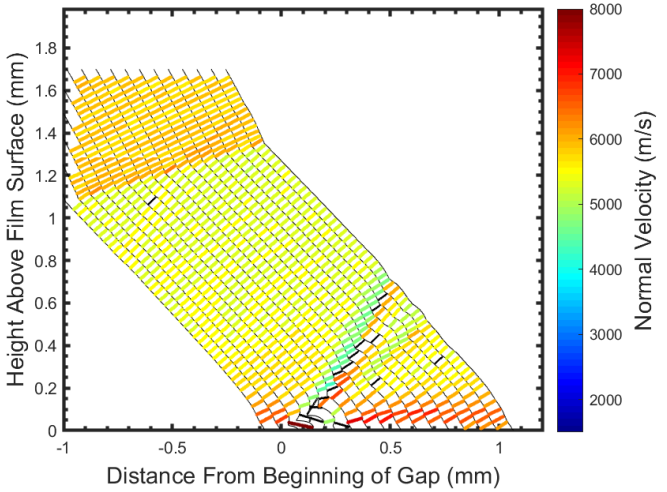

200 µm-thick film gap test with a 100 µm-gap-width.

Distance to steady-state state wave shape

- Detonation in film is seen in CGS images with a histogram shift.
- At t=1407 ns, film has already initiated and detonation propagates outward.
- At t=1418 ns, detonation emerges from film surface.
  - Detonation is significantly behind the air shock.
- At t=1425 ns, detonation catches up with air shock from initial film.

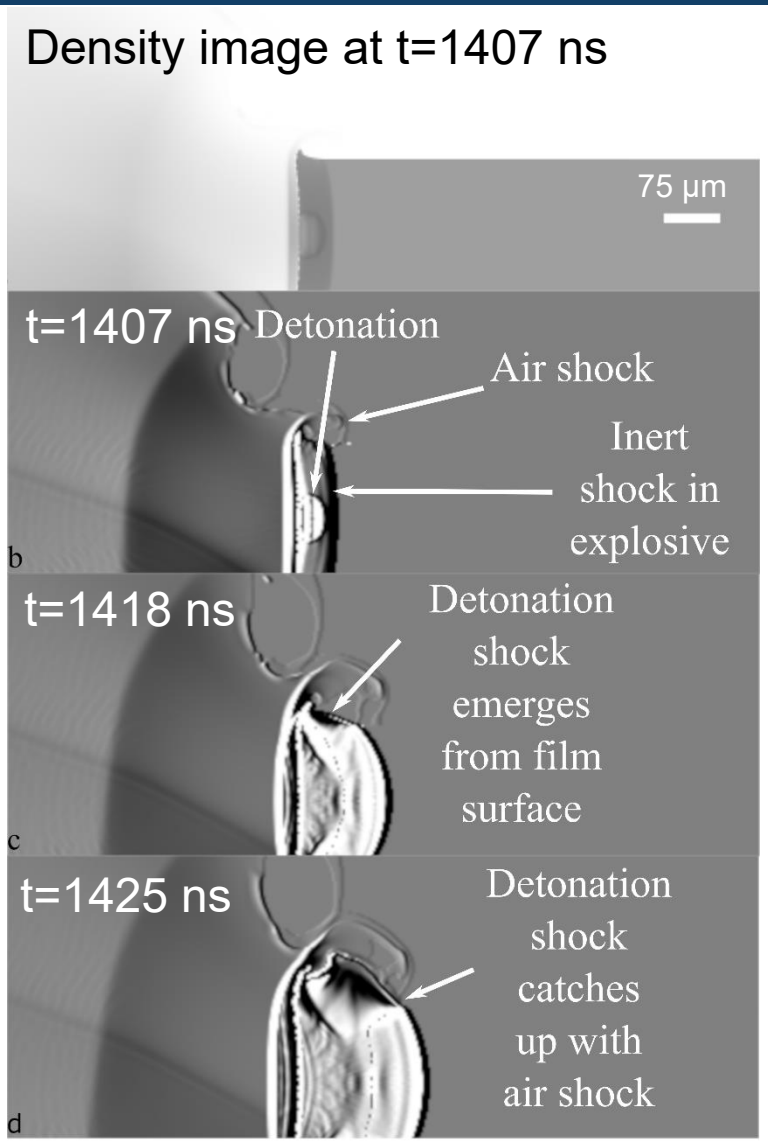

CTH infinite gap test

- There is a significant drop in velocity above and below the film height, that is not seen in experimental images.

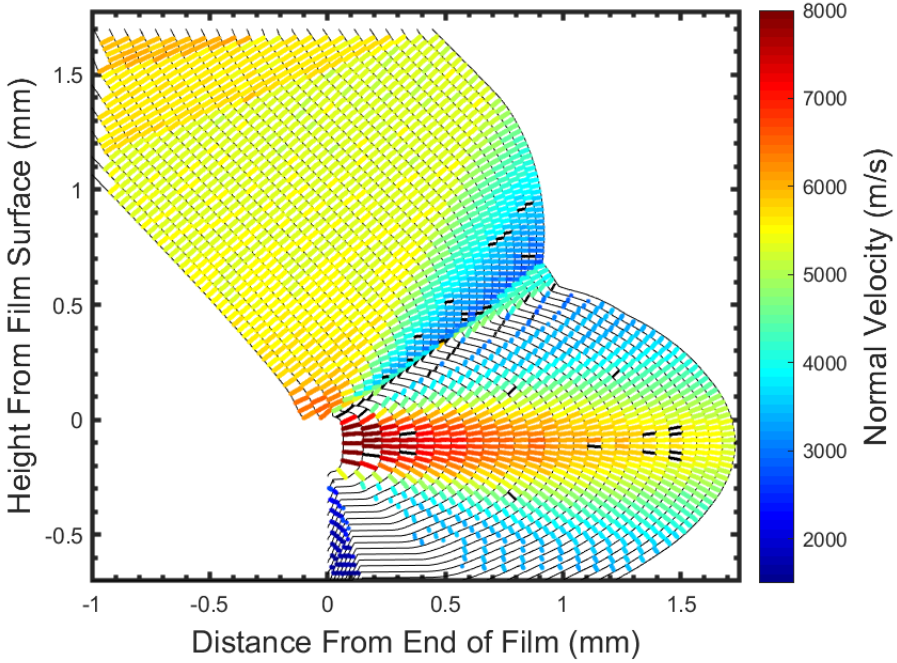

CTH infinite gap velocity plot.

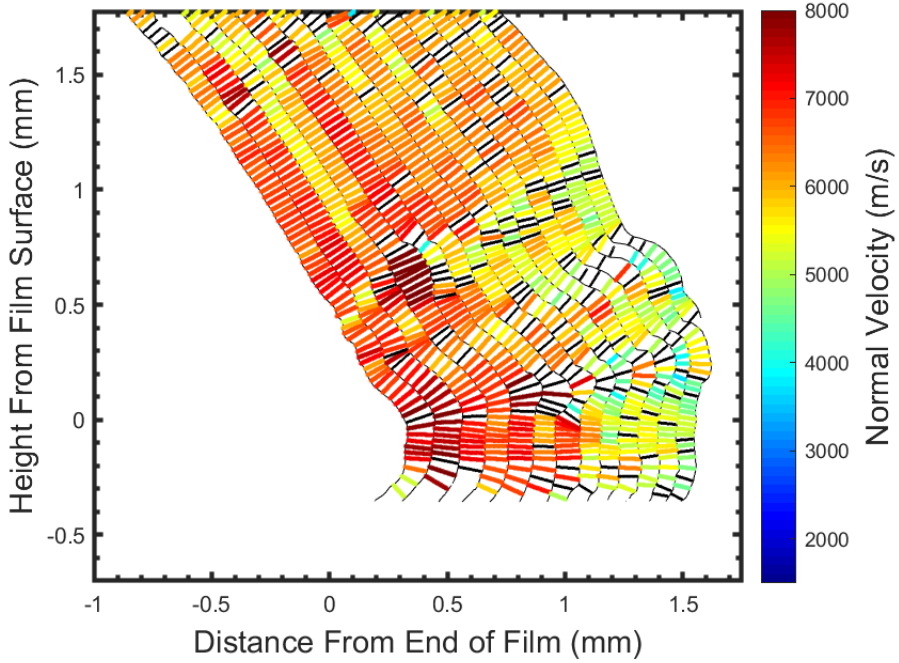

Experimental infinite gap velocity plot.

The trend between the CTH and experimental data matches fairly well.

- Computational data trend was slightly lower than trend of experimental data.
  - Expected since the 200 μm-thick PETN films in experiments had a higher detonation velocity than 200 μm-thick PETN films in simulations.

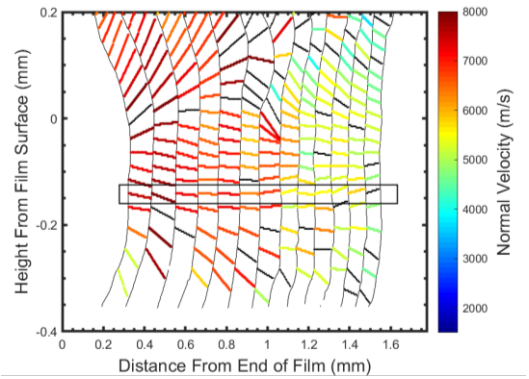

Experimental data

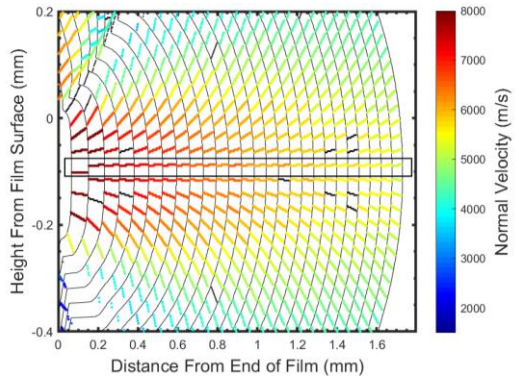

CTH data

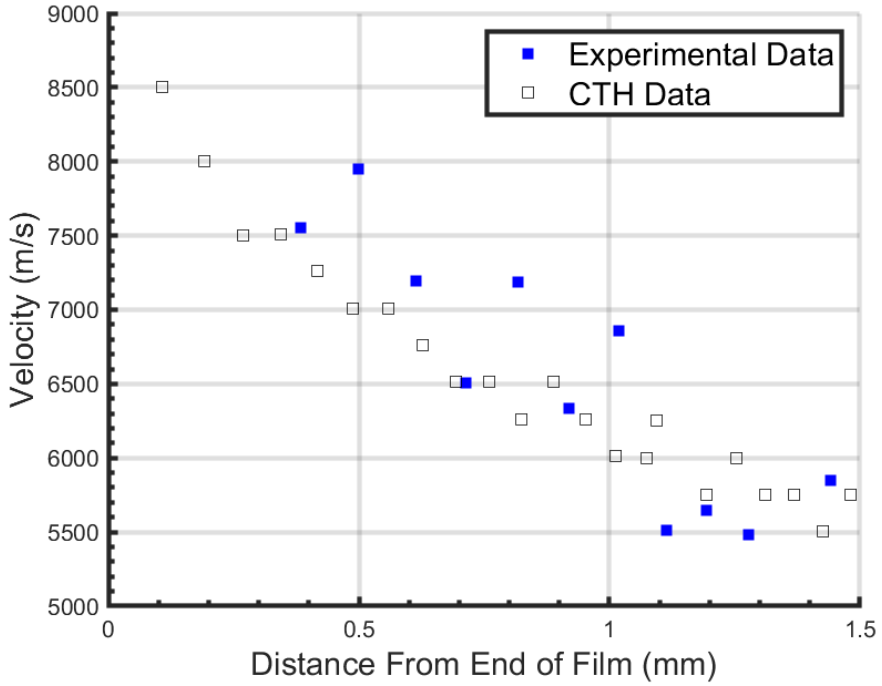

Experiments and computations were performed to visualize PETN films detonating across microcracks

- A new image processing algorithm was developed to:
  - Extract spatial data.
  - Quantify velocity:
    - Locally across dynamic wave shapes.
    - Of a pressure driven flow.
- CTH model provided further insight of experiments.
- As a result:
  - A critical gap width was determined.
  - Cracks were found to cause a large disturbance in the shock front.
    - Significantly larger than the crack itself.

Future work

- Perform statistical analysis to ascertain repeatability of gap test results.
- Develop an algorithm to calculate the average uncertainty in velocity found in the normal velocity plots.

Acknowledgements

I would like to thank my advisor Michael Hargather for shaping me into the researcher I am today. I would like to thank Eric Forrest for his tremendous support and feedback. Without them I would not have been able to complete this thesis. I would like to thank Bin Lim for serving on my committee. I would also like to thank Otis Solomon, Leanna Minier and Alex Tappan for the countless hours spent reviewing my work. I would like to thank Robert Knepper, Alex Tappan, Michael Marquez, Stephen Rupper, Jon Vasiliauskas and Caitlin O'Grady for their support with testing. I would also like to thank Cody Kirk for his great CTH advice. In addition I would like to thank Paul Shoemaker and Yolanda Moreno for starting the Campus Executive collaboration, that made this all possible.

I want to thank all the members of the Shock and Gas Dynamics Laboratory for making my time there enjoyable. Also for their great advice that helped me push my research further. I would like to thank my parents Julio and Christine for their endless support and encouragement.

Acknowledgements

This work was supported by the Laboratory Directed Research and Development program at Sandia National Laboratories, a multimission laboratory managed and operated by National Technology & Engineering Solutions of Sandia, LLC, a wholly owned subsidiary of Honeywell International, Inc., for the U.S. Department of Energys National Nuclear Security Administration under contract DE-NA0003525.

This report describes objective technical results and analysis. Any subjective views or opinions that might be expressed in the paper do not necessarily represent the views of the U.S. Department of Energy or the United States Government. Unclassified, unlimited release SAND2019-7499 PE

References

[1] Paul W. Cooper. *Explosives Engineering*. Wiley-VCH, 1996.

[2] Wildon Fickett and William C. Davis. *Detonation: Theory and Experiment*. Dove Publications, 2000.

[3] Herbert T. Knight and Douglas Venable. Apparatus for Precision Flash Radiograhpy of Shock and Detonation Waves in Gases. *Review of Scientific Instruments*, 29(2):92–98, 1958.

[4] John M. Densmore, Matthew M. Biss, Kevin L. McNesby, and Barrie E. Homan. High-Speed Digital Color Imaging Pyrometry. *Applied Optics*, 50(17):2659–2665, 2011.

[5] John M. McAfee, Blaine W. Asay, A. Wayne Campbell, and John B. Ramsay. Deflagration to Detonation in Granular HMX. Report No. LA-UR–91-2103, Los Alamos National Laboratory, 1991.

[6] Daniel H. Dolan. Foundations of VISAR Analysis. Report No. SAND2006-1950, Sandia National Laboratories, 2006.

[7] Kevin J. Fleming and Theresa A. Broyles. Shock Analysis Using the Multi Point Velocimeter (VISAR). Report No. SAND2003-3759, Sandia National Laboratories, 2003.

[8] L. M. Barker and R. E. Hollenbach. Laser Interferometer for Measuring High Velocities of any Reflecting Surface. *Journal of Applied Physics*, 43:4669–4675, 1972.

[9] O. T. Strand, D. R. Goosman, C. Martinez, and T. L. Whitworth. Compact System for High-Speed Velocimetry Using Heterodyne Techniques. *Review of Scientific Instruments*, 2006.

[10] V. Bouyer, M. Doucet, and L. Decaris. Experimental Measurements of the Detonation Wave Profile in a TATB Based Explosive. *EPJ Web of Conferences*, 10:00030, 2010.

[11] A. W. Campbell, M. E. Malin, T. J. Boyd Jr., and J. A. Hull. Precision Measurement of Detonation Velocities in Liquid and Solid Explosives. *The Review of Scientific Instruments*, 27(8):567–574, 1956.

[12] Wim Prinse, Rene van Esveld, Rene Oostdam, Murk van Rooijen, and Richard Bouma. Fibre-Optical Techniques for Measuring Various Properties of Shock Waves. *Proceedings of SPIE 3516, 23rd International Congress on High-Speed Photography and Photonics*, 1999.

[13] Jerry Benterou, Corey V. Bennett, Garrett Cole, D. E. Hare, Chadd May, Eric Udd, Stephen J. Mihailov, and Ping Lu. Embedded Fiber-Optic Bragg Grating (FBG) Detonation Velocity Sensor. *Proceedings of SPIE, Fiber Optic Sensors and Applications VI*, 7316:73160E, 2009.

[14] G. Rodriguez, R. L. Sandberg, Q. McCulloch, S. I. Jackson, S. W. Vincent, and E. Udd. Chirped Fiber Bragg Grating Detonation Velocity Sensing. *Review of Scientific Instruments*, 2013.

[15] Melvin A. Cook, Ray L. Doran, and Glen J. Morres. Measurement of Detonation Velocity by the Doppler Effect at Three-Centimeter Wavelength. *Journal of Applied Physics*, 26(4):426–428, 1954.

[16] A. W. Campbell and Ray Engelke. The Diameter Effect in High-Density Heterogeneous Explosives. In *Proceedings of the Sixth Symposium (International) on Detonation*, pages 642–651, Coronado, California, August 1976.

[17] Hartmut Badners and Carl-Otto Leiber. Method for the Determination of the Critical Diameter of High Velocity Detonation by Conical Geometry. *Propellants, Explosives, Pyrotechnics*, 17:77–81, 1992.

[18] B. M. Dobratz and P. C. Crawford. *LLNL Explosives Handbook*. 1985.

[19] Donna Price, A. R. Clairmont, and J. O. Erkman. The NOL Large Scale Gap Test . III. Compilation of Unclassified Data Suplementary Information for Interpretation of Results. Report No. NOLTR 74-40, Naval Ordnance Laboratory, 1974.

[20] Donna Price. Gap Tests and How They Grow. In *Minutes of the Explosives Safety Seminar (22nd)*, volume 1, pages 365–380, Aneheim, California, August 1986.

[21] Alexander S. Tappan. Microenergetics: Combustion and Detonation at Sub-Millimeter Scales. *AIP Conference Proceedings*, 955:997–1002, 2007.

[22] Alexander S. Tappan, Robert Knepper, Ryan R. Wixom, Jill C. Miller, Michael P. Marquez, and J. Patrick Ball. Critical Thickness Measurements in Vapor-Deposited Pentaerythritol Tetranitrate (PETN) and Films. In *14th International Detonation Symposium*, pages 1087–1095, Coeur d'Alene, Idaho, April 2010.

[23] Robert Knepper, Alexander S. Tappan, Ryan R. Wixom, and Mark A. Rodriguez. Controlling the Microstructure of Vapor-Deposited Pentaerythritol Tetranitrate Films. *Journal of Materials Research*, 26(13):1605–1613, 2011.

References (cont.)

[24] Donald M. Mattox. *Handbook of Physical Vapor Deposition (PVD) Processing*. Elsevier Inc., 2nd edition, 2010.

[25] Robert Knepper, Michael P. Marquez, and Alexander S. Tappan. Effects of Confinement on Detonation Behavior of Vapor-Deposited Hexanitroazobenzene Films. In *Proceedings of the 15th international detonation symposium*, San Francisco, California, July 2014.

[26] Robert Knepper, Ryan R. Wixom, Michael P. Marquez, and Alexander S. Tappan. Near-Failure Detonation Behavior of Vapor-Deposited Hexanitrostilbene (HNS) Films. *AIP Conference Proceedings*, 1793:030014, 2017.

[27] Ryan R. Wixom, Alexander S. Tappan, Gregory T. Long, Anita M. Renlund, Eric J. Welle, Joel P. Mcdonald, Bradley H. Jared, Aaron L. Brundage, and Joseph R. Michael. Microenergetics: Characterization of Sub-Millimeter PETN Films. In *35th International Pyrotechnics Seminar and Symposium*,, pages 181–192, Ft. Collins, Colorado, July 2008.

[28] U. S. Department of Energy. DOE Standard Explosives Safety. Report No. DOE-STD-1212-2012, Washington, DC, June 2012.

[29] Henry Eyring, Richard E. Powell, George H. Duffey, and Ransom B. Parlin. The Stability of Detonation. *Chemical Reviews*, 45(1):69–181, 1948.

[30] A. W. Campbell, W. C. Davis, J. B. Ramsay, and J. R. Travis. Shock Initiation of Solid Explosives. *The Physics of Fluids*, 4:511–521, 1961.

[31] P. Howe, R. Frey, B. Taylor, and V. Boyle. Shock Initiation and the Critical Energy Concept. In *Proceedings of the 6th symposium (international) on detonation*, Coronado, California, August 1976.

[32] B. A. Khasainov, B. S. Ermolaev, H. N. Presles, and P. Vidal. On the Effect of Grain Size on Shock Sensitivity of Heterogeneous High Explosives. In *Shock Waves*, volume 7, pages 89–105, 1997.

[33] Alexander S. Tappan, Ryan R. Wixom, and Robert Knepper. Geometry Effects on Detonation in Vapor-Deposited Hexanitroazobenzene (HNAB). *AIP Conference Proceedings*, 1793:030036, 2017.

[34] Alexander S. Tappan, Anita M. Renlund, Gregory T. Long, Stanley H. Kravitz, Kenneth L. Erickson, Wayne M. Trott, and Melvin R. Baer. Microenergetic Processing and Testing to Determine Energetic Material Properties at the Mesoscale. In *12th International Detonation Symposium*, San Diego, California, August 2002.

[35] Omkar A. Nafday, Rajasekar Pitchimani, and Brandon L. Weeks. Patterning High Explosives at the Nanoscale. *Propellants, Explosives, Pyrotechnics*, (5), 2006.

[36] Alexander S. Tappan, Robert Knepper, Ryan R. Wixom, Michael P. Marquez, J. Patrick Ball, and Jill C. Miller. Critical Detonation Thickness in Vapor-Deposited Pentaerythritol Tetranitrate (PETN) Films. *AIP Conference Proceedings*, 1426:677–680, 2012.

[37] Terry R. Gibbs and Alphonse Popolato, editors. *LASL Explosive Property Data*. University of California Press, Ltd., 1980.

[38] John Starkenberg and Toni M. Dorsey. An Assessment of the Performance of the History Variable Reactive Burn Explosive initiation Model in the CTH Code. Report No. ARL-TR-1667, Army Research Laboratory, 1998.

[39] Eric C. Forrest, Robert Knepper, Michael T. Brumbach, Kim Archuleta, Michael P. Marquez, Hy D. Tran, and Alexander S. Tappan. Influence of Surface Contamination on the Microstructure and Morphology of Vapor-Deposited Pentaerythritol Tetranitrate (PETN) Films. In *APS Topical Conference on the Shock Compression of Condensed Matter*, St. Louis, Missouri, July 2017.

[40] Robert Knepper, Eric C. Forrest, Michael P. Marquez, and Alexander S. Tappan. Effect of Microstructure on the Detonation Behavior of Vapor-Deposited Pentaerythritol Tetranitrate (PETN) Films. *AIP Conference Proceedings*, 1979:150022, 2018.

[41] M. D. Thouless. Combined Buckling and Cracking of Films. *Journal of the American Ceramic Society*, 76(11):2936–2938, 1993.

[42] Eric C. Forrest, Julio C. Peguero, Michael J. Hargather, Robert Knepper, Alexander S. Tappan, Michael P. Marquez, Jonathan G. Vasiliauskas, and Stephen G. Rupper. Effect of Microscale Defects on Shock and Detonation Propogation in Pentaerythritol Tetranitrate (PETN) Films. In *Proceedings of the 16th International Detonation Symposium*, 2018.

[43] Gary S. Settles. *Schlieren and Shadowgraph Techniques*. Springer-Verlag, 2001.

[44] Michael J. Hargather and Gary S. Settles. Optical Measurement and Scaling of Blasts from Gram-Range Explosive Charges. *Shock Waves*, 17:215–223, 2007.

[45] Michael J. Hargather. *Scaling, Characterization, and Application of Gran-Range Explosive Charges To Blast Testing of Materials*. PhD thesis, The Pennsylvania State University, 2008.

[46] F. R. Svingala, M. J. Hargather, and G. S. Settles. Optical Techniques for Measuring the Shock Hugoniot Using Ballistic Projectile and High-Explosive Shock Initiation. *International Journal of Impact Engineering*, pages 76–82, 2012.

[47] Mark Lieber, Michael Murphy, and Matthew Biss. On a Physics-Based Model Equation for Shock-Position Evolution in PMMA. *AIP Conference Proceedings*, 1979:160014, 2018.

References (cont.)

[48] M. J. Murphy and C. E. Johnson. Preliminary Investigations of HE Performance. In *Journal of Physics: Conference Series*, 2014.

[49] Matthew Biss, Michael Murphy, and Mark Lieber. Qualification of a Multi-Diagnostic Detonator-Output Characterization Procedure Utilizing PMMA Witness Blocks. *AIP Conference Proceedings*, 1979:160005, 2018.

[50] S. A. Clarke, C. A. Bolme, M. J. Murphy, C. D. Landon, T. A. Mason, R. J. Adrian, A. A. Akinci, M. E. Martinez, and K. A. Thomas. Using Schlieren Visualization to Track Detonator Performance. *AIP Conference Proceedings*, 955:1089–1092, 2007.

[51] Kyle O. Winter and Michael J. Hargather. Three-Dimensional Shock Wave Reconstruction Using Multiple High-Speed Digital Cameras and Background-Oriented Schlieren Imaging. *Experiments in Fluids*, 60:93, 2019.

[52] M. N. Skaggs, M. J. Hargather, and M. A. Cooper. Characterizing Pyrotechnic Igniter Output with High-Speed Schlieren Imaging. *Shock Waves*, 27:15–25, 2017.

[53] Charles E. Anderson Jr. An Overview of the Theory of Hydrocodes. *International Journal of Impact Engineering*, pages 33–59, 1987.

[54] David J. Benson. Computational Methods in Lagrangian and Eulerian Hydrocodes. *Computer Methods in Applied Mechanics and Engineering*, 1992.

[55] Ralph Menikoff. On Beyond the Standard Model for High Explosives Challenges and Obstacles to Surmount. *AIP Conference Proceedings*, 1195:18–25, 2010.

[56] Ralph Menikoff and Christina A. Scovel. Systematic Approach to Verification and Validation: High Explosive Burn Models. Report No. LA-UR-12-20591, Los Alamos National Laboratory, 2012.

[57] John Starkenberg. Modeling Detonation Propagation and Failure Using Explosive Initiation Models in a Conventional Hydrocode. In *12th International Detonation Symposium*, San Diego, California, August 2002.

[58] William Von Holle and Charles Martin. Safe Handling of Insensitive High Explosive Weapon Subassemblies at the Pantex Plant. Report No. DNFSB/TECH-24, Defense Nuclear Facilities Safety Board, 1999.

[59] Brendan M. Welch, James E. Fritz, and Steven L. Perkins. Explosive Systems Development Using Hydrocode Modeling. In *American Institute of Aeronautics and Astronautics 33rd Joint Propulsion Conference and Exhibit*, Seattle, Washington, July 1997.

[60] L. Vitos, A. V. Ruban, H. L. Skriver, and J. Kolair. The Surface Energy of Metals. *Surface Science*, (Denmark), 1998.

[61] W. R. Tyson and W. A. Miller. Surface Free Energies of Solid Materials Estimation From Liquid Surface Tension Measurements. *Surface Science*, 1977.

[62] Justin Peatross and Michael Ware. *Physics of Light and Optics*. 2015.

[63] www.newport.com/n/focusing-and-collimating.

[64] John Canny. A Computational Approach to Edge Detection. *IEEE Transactions on Pattern Analysis and Machine Intelligence*, PAMI-8(6):979–698, November 1986.

[65] Karel Zuiderveld. Contrast Limited Adaptive Histograph Equalization. *Graphic Gems IV*, 1994.

[66] Steven C. Chapra and Raymond P. Canale. *Numerical Methods for Engineers*. McGraw-Hill Education, 2015.

[67] E. L. Lee, H. C. Hornig, and J. W. Kury. Adiabatic Expansion of High Explosive Detonation Products. Report No. UCRL-50422, Lawrence Livermore National Laboratory, 1968.

[68] Michael E. Berger. Detonation of High Explosives in Lagrangian Hydrodynamic Codes Using the Programmed Burn Technique. Report No. LA-6097-MS, Los Alamos National Laboratory, 1975.

[69] Sesame: The Los Alamos National Laboratory Equation of State Database. Report No. LA-UR-92-3407, Los Alamos National Laboratories, 1992.

[70] J. M. McGlaun and S. L. Thompson. CTH: A Three-Dimensional Shock Wave Physics Code. *International Journal of Impact Engineering*, 10:351–360, 1990.

[71] Rafael C. Gonzalez, Richard E. Woods, and Steven L. Eddins. *Digital Image Processing Using MATLAB*. Gatesmark Publishing, 2nd edition, 2009.

[72] J. B. Ramsay and A. Popolato. Analysis of Shock Wave and Initiation Data for Solid Explosives. In *Proceedings of the Fourth International Symposium on Detonation*, White Oak Maryland, October 1965.

[73] William C. Davis. Shock Desensitizing of Solid Explosive. In *Proceedings of the 14th International Detonation Symposium*, Coeur d'Alene , Idaho, April 2010.

Backup Slides

Gap Test Failure Tables

70 µm-thick film failure table

Film Thickness (µm)	Gap Width (µm)	Detonation Propagation	Substrate
70	0	No	Oxidized Al
70	0	No	Bare Al
70	10	No	Oxidized Al
70	10	No	Bare Al
70	25	No	Oxidized Al
70	25	No	Bare Al
70	50	No	Oxidized Al
70	50	No	Bare Al

200 µm-thick film failure table

Film Thickness (µm)	Gap Width (µm)	Detonation Propagation
200	25	Yes
200	25	Yes
200	25	Yes
200	25	Yes
200	25	Yes
200	50	Yes
200	50	Yes
200	75	Yes
200	75	Yes
200	80	Yes
200	75-120	Yes
200	93	No
200	95	No
200	100	No
200	110	Yes
200	110	No
200	170	No

Note: the film with the gap width of 75-120 µm is due to a rough edge.

400 µm-thick film failure table

Film Thickness (µm)	Gap Width (µm)	Detonation Propagation
400	80	Yes
400	100	Yes
400	125	Yes
400	160	Yes
400	180	Yes
400	180	Yes
400	200	Yes
400	200	No
400	220	yes

Rounded Edges of PETN Films

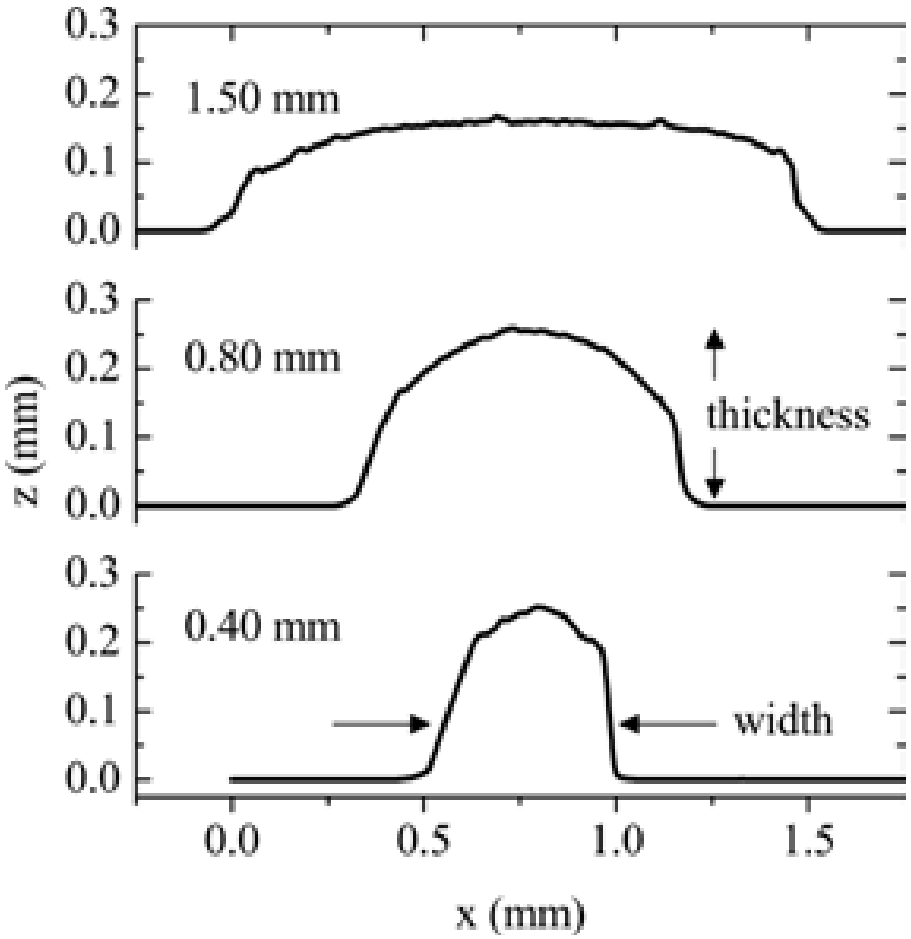

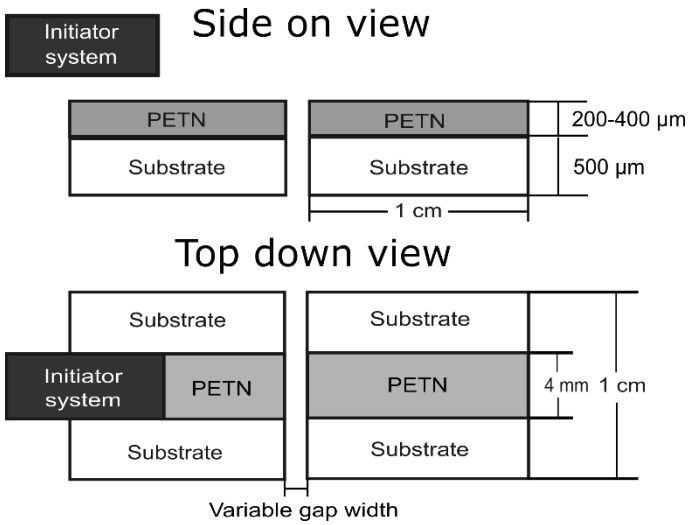

Surface profilometer measurements of PETN films deposited at various widths [Tappan 2010]. The view is from the front.

Computation of the Derivative of the Density Field

- A center difference numerical derivative can be performed with the equation shown.
- Spatial Filtering [Gonzalez 2009] can be used to perform the numerical derivative.
- Spatial filtering is performed by applying a mask composed of multiplication factors, C_i, to a region of pixels on the image.
- Applying the mask shown on the bottom yields the same answer as the numerical derivative shown above.

$$\frac{dx}{dy} = \frac{x_{n+h} - x_{n-h}}{2h}$$

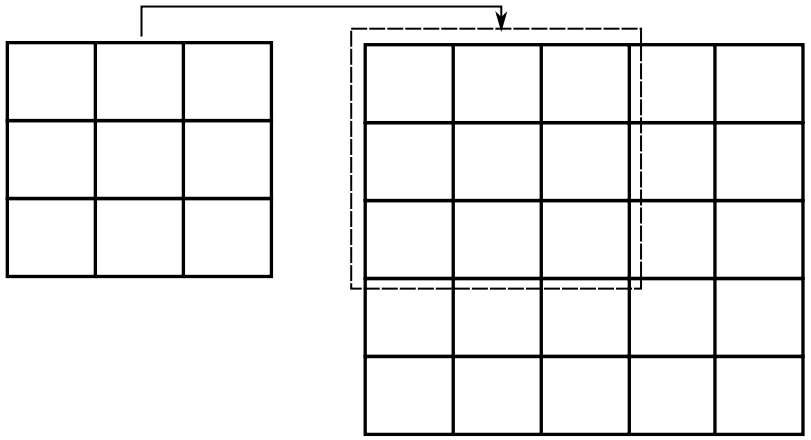

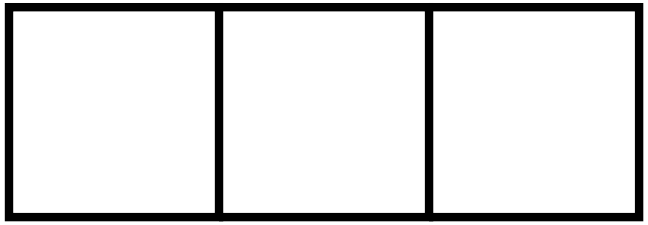

Unconfined PETN Critical Detonation Thickness

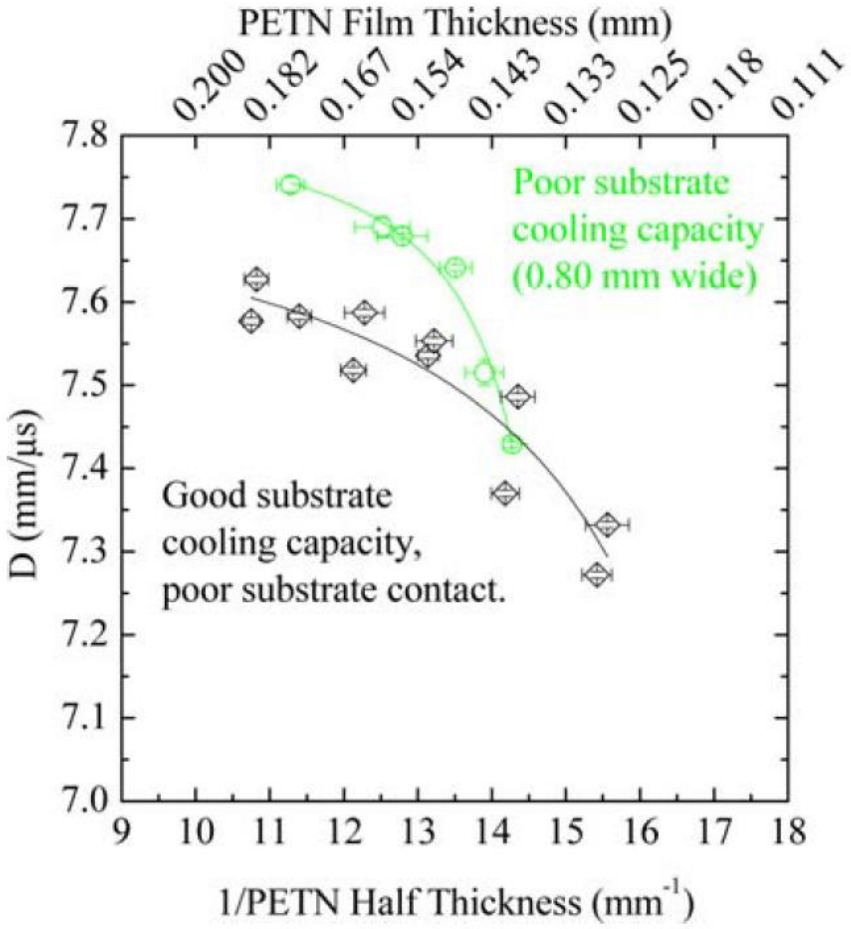

[Tappan2012]

Detonation is a rapid combustion driven by shock

- A chemical reaction in an explosive is initiated by a shock wave propagating through the explosive.
- The energy produced by this chemical reaction drives the shock front and thus the detonation.

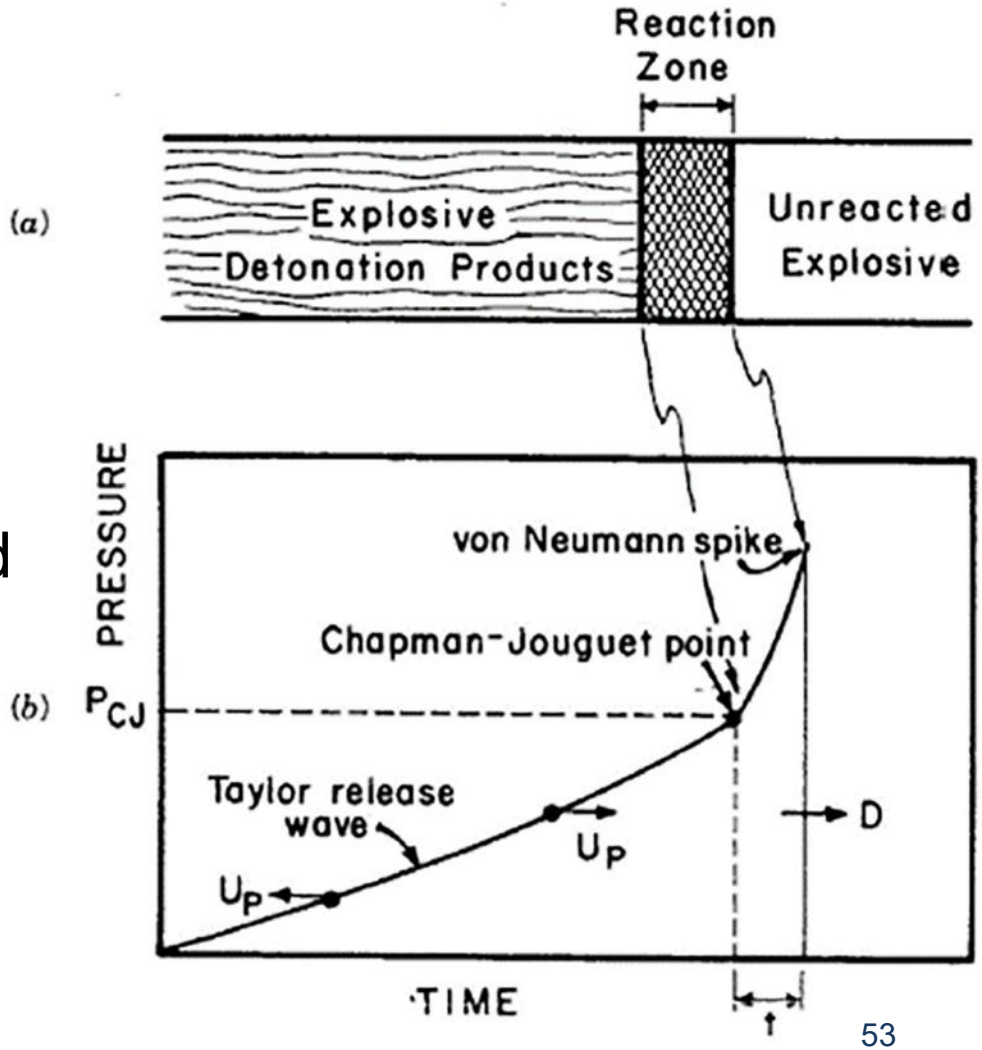

Burn Rate Calibration

- The burn models are typically calibrated with shock-to-detonation experiments, such as the wedge test [Menikoff2010,Starkenberg2002].
- The wedge test is used to determine the run distance versus input pressure.
- The run distance is the length an input pressure needs to travel before initiation.

Mesh resolution was 8000 x 2000 cells.

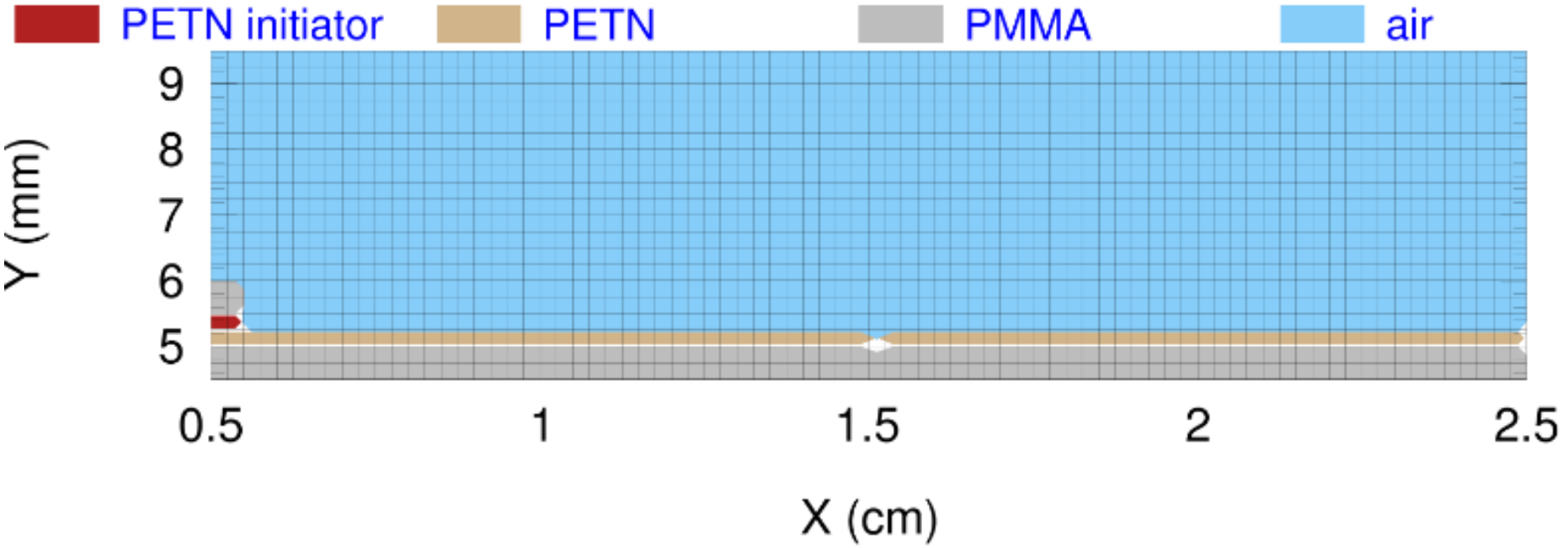

2D model with 80 x 20 mesh grid overlay. Each cell represents a 100 x 100 cell grid.